CAPITAL UNIVERSITY OF SCIENCE AND TECHNOLOGY, ISLAMABAD

A Hybrid Nanofluid Flow under the Influence of Cattaneo-Christov Heat Flux Model and Activation Energy

by

Ramsha Khalid

A thesis submitted in partial fulfillment for the degree of Master of Philosophy

in the

Faculty of Computing
Department of Mathematics

2024

This thesis is dedicated to my cherished parents, whose boundless love, unwavering support and belief in my abilities have been the driving force behind my academic journey. Their sacrifices, encouragement, and constant presence have inspired me to persevere and reach for excellence. I am forever grateful for the values and guidance they have instilled in me, which have shaped my character and ambitions. This work is a testament to their selfless dedication and the profound impact they have had on my life. I am privileged to have such remarkable parents who have always stood by me with unwavering love and care.

CERTIFICATE OF APPROVAL

The Influence of Cattaneo-Christov Heat Flux Model and Activation Energy on Hybrid Nanofluid Flow

by

Ramsha Khalid

(MMT213025)

THESIS EXAMINING COMMITTEE

(a)	External Examiner	Dr. Rashid Mahmood	Air University, Islamabad
(b)	Internal Examiner	Dr. Samina Rashid	CUST, Islamabad
(c)	Supervisor	Dr. Muhammad Sagheer	CUST, Islamabad

Dr. Muhammad Sagheer
Thesis Supervisor
September, 2024

Dr. Muhammad Sagheer
Head
Dept. of Mathematics
September, 2024

Dr. Muhammad Abdul Qadir
Dean
Faculty of Computing
September, 2024

Author's Declaration

I, **Ramsha Khalid** hereby state that my MPhil thesis titled "**The Influence of Cattaneo-Christov Heat Flux Model and Activation Energy on Hybrid Nanofluid Flow**" is my own work and has not been submitted previously by me for taking any degree from Capital University of Science and Technology, Islamabad or anywhere else in the country/abroad.

At any time if my statement is found to be incorrect even after my graduation, the University has the right to withdraw my MPhil Degree.

(Ramsha Khalid)

Registration No: MMT213025

Plagiarism Undertaking

I solemnly declare that research work presented in this thesis titled "**The Influence of Cattaneo-Christov Heat Flux Model and Activation Energy on Hybrid Nanofluid Flow**" is solely my research work with no significant contribution from any other person. Small contribution/help wherever taken has been duly acknowledged and that complete thesis has been written by me.

I understand the zero tolerance policy of the HEC and Capital University of Science and Technology towards plagiarism. Therefore, I as an author of the above titled thesis declare that no portion of my thesis has been plagiarized and any material used as reference is properly referred/cited.

I undertake that if I am found guilty of any formal plagiarism in the above titled thesis even after award of MPhil Degree, the University reserves the right to withdraw/revoke my MPhil degree and that HEC and the University have the right to publish my name on the HEC/University website on which names of students are placed who submitted plagiarized work.

(Ramsha Khalid)

Registration No: MMT213025

Acknowledgement

I would like to express my deepest gratitude and appreciation to all those who have encouraged to the successful completion of this thesis.

First and foremost, I am immensely grateful to my supervisor, Dr. Muhammad Sagheer, for his devoted guidance, encouragement, and support throughout this research journey. His expertise and valuable insights have been instrumental in shaping the direction and quality of this work.

I am also deeply grateful to my mother and sister for their presistent love, encouragement, and belief in me. Their constant support and understanding have been a source of strength during the challenging moments of this academic pursuit. Their sacrifices and words of encouragement have kept me motivated and focused.

A special note of thanks goes to my father, whose boundless love, encouragement, and sacrifices have been the bedrock of my academic journey. His unwavering belief in me has been a driving force behind my achievements, and I am forever grateful for his guidance and wisdom.

In conclusion, this thesis would not have been possible without the collective efforts of all those mentioned above.

(Ramsha Khalid)

Registration No: MMT213025

Abstract

Theoretical and numerical analysis of Cattaneo-Christov heat flux model, magnetohydrodynamic and impact of thermal radiation on hybrid nanofluid flow at a stagnation point over a stretching permeable sheet has been carried out through the utilization of the shooting method. By incorporating the Cattaneo-Christov heat flux model, the governing equations are formulated and analyzed, and shooting method is employed to effectively solve the transformed ordinary differential equations. The research prominently identifies the crucial influence of the Cattaneo-Christov heat flux and magnetic field effects on heat transfer efficiency, which in turn enhances thermal radiation in the system. Additionally, incorporating unsteadiness and the shrinking parameter significantly impacted the velocity, temperature, and concentration profiles, as well as their rates of change. The study indicates that nanoparticle concentration exhibits initial fluctuations before stabilizing with certain parameter combinations. This transient behavior is important for understanding the dynamics of nanofluid flow and its engineering applications.

Contents

List of Figures

List of Tables

Abbreviations

BCs	Boundary conditions
HNF	Hybrid nanofluid
IVPs	Initial value problem
MHD	Magnetohydrodynamics
NF	Nanofluid
ODEs	Ordinary differential equation
PDEs	Partial differential equation
RK-4	Runge-Kutta method of order 4

Symbols

u, v	Velocity components
μ	Viscosity
ν	Kinematic viscosity
ρ	Density
B_o	Magnetic field strenght
T	Temperature of nanoparticles
K	Thermal conductivity
ρc_p	Heat capacity
T_∞	Ambient temperature of fluid
C	Concentration
C_f	Nanoparticles concentration at the stretching surface
C_∞	Ambient concentration
q_r	Radiative heat flux
B_o	Magnatic field constant
σ^*	Stefan Boltzmann constant
k^*	Absorption coefficient
η	Similarity variable
$f(\eta)$	Dimensionless velocity
$\theta(\eta)$	Dimensionless temperature
$\phi(\eta)$	Dimensionless concentration
Q_o	Heat source
h_f	Cofficient of heat transfer
M	Magnetic field parameter
Nt	Thermophoresis motion parameter

Pr	Prandtl number
Nb	Brownian motion parameter
Q	Heat source
D_B	Brownian motion
D_T	Thermophoresis diffusion coefficient
Re	Reynolds number
Re_x	Local Reynolds number
Nu	Nusselt number
Nu_x	Local Nusselt number
C_f	Skin friction coefficient
m	Fitted rate constant
K_1	Boltzmann constant
C_r	Reaction rate parameter
δ_T	Thermal relaxation parameter
θ_w	Temprature ratio parameter
E	Activation energy parameter
E_a	Activation energy coefficient
β_T	Heat flux relaxation parameter

Subscripts

p	Nanoparticle
nf	Nanofluid
hnf	Hybrid nanofluid

Chapter 1

Introduction

1.1 Background

Now a days, a familiar research area is the analysis of hybrid nanofluid. Choi [1] originally proposed various nanofluids that contain unique types of nanoparticles.Tiwari and Das [2] reported some basic models and fundamental applications for studying nanofluids. Many mathematicians have thought about using highly thermally conductive liquids, for example, Safaei et al. [3] investigated the cooling of electronics using nanofluids. Hybrid nanofluids are made up of two or more solid nanoparticles suspended in any base liquid. A development of nanofluids is hybrid nanofluids. Compared to regular nanoliquids, these nanofluids have significantly better heat transfer capabilities. Hybrid nanofluids have uses in machine heat transfer coolants, electromechanical systems, optical sensors, and the field of nanomedicine.

Research efforts have intensified to optimize heat transfer by utilizing hybrid nanofluids. The concept was initially introduced by Suresh et al.[4]. Waini et al.[5] investigated micropolar hybrid nanofluid flow, considering viscous dissipation near a moving plate. Additionally, Sharma et al. [6] utilized molybdenum disulphide (MoS_2) and alumina nanoparticles in an oil-water mixture to illustrate the development of a hybrid nanofluid. Nadeem et al. [7] investigated the dynamics of hybrid nanofluid flow around a stagnant point in a cylindrical configuration.

Furthermore, the research by Chamkha et al. [8] focused on the dynamics of heat transfer in a rotating hydromagnetic flow system with a hybrid nanofluid.

Khan et al. [9] investigated convective Marangoni flow in a hybrid nanofluid consisting of $MnZiFe_2O_4 - NiZnFe2O_4/H_2O$, assuming a stretchable surface with a Darcy -Forchheimer medium. The study by Nadeem and Abbas [10] explored a hydromagnetic flow problem in a micropolar hybrid nanofluid near a circular cylinder, taking slip effects into account. Additionally, the research by Subhani and Nadeem [11] involved a comparative analysis of micropolar nanofluid and micropolar hybrid nanofluid. Izady et al. [12] investigated the magnetohydrodynamics (MHD) boundary layer flow mechanism in a hybrid Fe_2O_3CuO/H_2O nanofluid affected by thermal radiation from a shrinking/stretchable wedge. In their research, Jabbaripour et al. [13] investigated the influence of a magnetic field on the steady-state flow induced by a circular wavy cylinder, employing a water-based hybrid nanofluid comprising aluminum and copper nanoparticles. Xia et al. [14] researched the mixed convective flow characteristics of a hybrid micropolar nanofluid, focusing on the impacts of microorganisms and multiple slip conditions. It was noted that an elevated Hartmann number leads to a decline in the flow velocity of the hybrid nanofluid.

Boundary layer flow problems arising from shrinked or stretched sheets have significant real-world applications across various industrial and technical fields, including hot rolling, glass fiber manufacturing, extrusion processes, and more. Initially, Crane [15] examined the behavior of fluid flow over a stretchable sheet and provided a closed-form solution to the problem. Subsequently, research in the area of shrinking or stretching sheets has expanded. Munawar et al. [16] contributed to this field by developing a precise solution for the flow problem considering slip effects between two stretching plates. Waini et al. [17] explored the unsteady flow and heat transfer processes in a hybrid nanofluid contained within a stretched/shrunk sheet. Meanwhile, Manjunatha et al. [18] focused on studying hybrid nanofluids to investigate the consequences of inconsistent viscosity on the boundary layer flow past a stretchable surface.

Miklavcic and Wang [19] investigated the behavior of steady flow over a shrinking

sheet, highlighting how crucial mass suction is in shaping the flow characteristics around the shrinking sheet. The study by Tie-Gang et al. ([20]) elucidated how viscous time-dependent fluid flow behaves around a shrinking sheet. The studies conducted by Fang ([21]) and later by Fang and Zhang ([22]) investigated the boundary layer flow mechanism, underscoring the importance of power-law velocity distributions. Rohni et al. [23] explored the heat transfer and flow mechanism facilitated by a shrinking sheet, taking into account the effects of suction in nanofluids.

Scientists and researchers are very interested in studying how magnetic fields affect fluid dynamics because of their many practical uses, including in Helmholtz coils, magnetic levitation, Teltron tubes, Maxwell coils, and electric dynamos. The experiments by Abel et al. [24] focused on examining hydromagnetic flow and heat transfer mechanisms on a stretchable surface, while Ibrahim et al. [25] studied the heat transfer behavior of nanofluids near stagnant points under the influence of magnetic fields. Abbas et al. [26] also examined the flow scenario involving a hybrid nanofluid composed of $Ag - Ni$ mixed with water.

Research on hybrid nanofluid flow using the Cattaneo-Christov heat flux model combined with a concentrated profile has not been conducted before. This study aims to fill this gap, providing new and valuable insights that enhance the current understanding in the field. Similarity transformations are used in the study to convert nonlinear partial differential equations into dimensionless ordinary differential equations, and the shooting method was applied to obtain the results. Numerical results were generated and visualized graphically with MATLAB. The tables and graphs clearly illustrate the impact of significant parameters on the velocity f(η), temperature $\theta(\eta)$, and concentration profile $\phi(\eta)$.

1.2 Thesis Structure

Chapter 2 serves as an introduction to the thesis and provides essential definitions and terminologies that are crucial for understanding the concepts discussed in

subsequent chapters. This chapter aims to establish a foundational understanding of the key terms and concepts that will be used throughout the thesis.

Chapter 3 presents a thorough numerical examination of the MHD stagnation point flow of HNF $Al_2O_3 - Cu/H_2O$ over a stretched permeable sheet in the cylindrical polar coordinate system r and z. The proposed numerical model incorporates heat and mass transfer phenomena across the stretched permeable sheet. To obtain the numerical outcomes of the governing flow equations, the shooting technique is utilized. This chapter explores the flow characteristics and heat transfer performance of the $Al_2O_3 - Cu/H_2O$ hybrid nanofluid under various operating conditions.

Building upon the model discussed in Chapter 3, **Chapter 4** extends the investigation to a water-based hybrid nanofluid ($Al_2O_3 - Cu/H_2O$). In this chapter, we introduce Cattaneo-Christov heat flux, into the energy equation of the present model. Additionally, we include the concentration equation for the hybrid nanofluid in the proposed model.

Chapter 5 presents the concluding remarks and underscores the significant findings from the research conducted in this thesis. It aims to provide a thorough summary of the study's main outcomes and contributions .

The **Bibliography** section offers a detailed list of all references and sources utilized in the thesis. It recognizes the contributions of prior research and upholds the academic integrity of the work by appropriately crediting the original authors and sources.

Chapter 2

Preliminaries

In this chapter, we will elucidate fundamental definitions, essential laws, terminologies, and key concepts necessary for the analysis of nonlinear partial differential equations. These foundational elements are crucial for comprehending the subsequent chapters of this thesis and will provide a solid framework for the development of a comprehensive understanding.

2.1 Foundational Concepts

2.1.1 Fluid

"A substance in the liquid or gas phase is referred to as a fluid. Distinction between a solid and a fluid is made on the basis of the substances ability to resist an applied shear (or tangential) stress that to change its shape. A solid can resist an applied shear stress by deforming, whereas a fluid deforms continuously under the influence of shear stress no matter how small." [27]

2.1.2 Fluid Dynamics

"Fluid dynamics is the study of the motion of liquids, gases and plasma from one place to another." [28]

2.1.3 Fluid Mechanics

"Fluid mechanics is that branch of science which deals with the behavior of the fluid (liquids or gases) at rest as well as in motion." [28]

2.1.4 Magnetohydrodynamics

"Magnetohydrodynamics (MHD) is concerned with the flow of electrically conducting fluids in the presence of magnetic fields, either externally applied or generated within the fluid by inductive action."[28]

2.1.5 Viscosity

"Viscosity is defined as the property of a fluid which offers resistance to the movement of one layer of fluid over another adjacent layer of the fluid. Mathematically,

$$\mu = \frac{\tau}{\frac{\partial u}{\partial y}},$$

where μ is viscosity coefficient, τ is shear stress and $\frac{\partial u}{\partial y}$ represents the velocity gradient." [28]

2.1.6 Kinematic Viscosity

"Kinematic viscosity is defined as the ratio between the dynamic viscosity and density of fluid. It is denoted by the Greek symbol ν, thus mathematically,

$$\nu = \frac{\text{Viscosity}}{\text{Density}} = \frac{\mu}{\rho}$$

where the unit of kinematic viscosity is m^2/sec ." [28]

2.2 Classification of Fluid

2.2.1 Ideal Fluid

"A fluid which is incompressible and is having no viscosity, is known as an ideal fluid. Ideal fluid is only an imaginary fluid as all the fluids, which exist, have some viscosity." [28]

2.2.2 Newtonian Fluid

"A real fluid, in which shear stress is directly, proportional to the rate of shear strain (or velocity gradient), is known as a Newtonian fluid." [28]

2.2.3 Non-Newtonian Fluid

"A real fluid, in which the shear stress is not proportional to the rate of shear strain (or velocity gradient), is known as a Non-Newtonian fluid." [28]

2.3 Modes of Heat Transfer

2.3.1 Conduction

"The transfer of heat within a medium due to a diffusion process is called conduction. The Fourier heat conduction law states that the heat flow is proportional to the temperature gradient." Examples are during the ironing process, heat is transferred from the iron to the fabric. Chocolate candy in a hand will eventually melt as heat is conducted from a hand to the chocolate. [29]

2.3.2 Radiation

"Thermal radiation is defined as radiant (electromagnetic) energy emitted by a medium and is solely to the temperature of the medium".

Examples are microwaves from an oven, X rays from an X-ray tube and ultraviolet light from the sun.[29]

2.3.3 Convection

"The mode by which heat is transferred between a solid surface and the adjacent fluid in motion when there is a temperature difference between the two is known as convection heat transfer. The temperature of the fluid stream refers either to its bulk or free stream temperature."[29]

2.4 Different Flow Classifications

2.4.1 Steady Flow

"Steady flow is defined as that type of flow in which the fluid characteristics like velocity, pressure, density, etc., at a point do not change with time. Mathematically, for steady flow

$$\frac{\partial Q}{\partial t} = 0,$$

where Q is any fluid property." [29]

2.4.2 Unsteady Flow

"Unsteady flow is defined as that type of flow in which the fluid characteristics like velocity, pressure, density, etc., at a point do change with time. Mathematically, for unsteady flow

$$\frac{\partial Q}{\partial t} \neq 0,$$

where Q is any fluid property." [29]

2.4.3 Compressible and Incompressible Flows

"Compressible flow is that type of flow in which the density for the fluid changes from point to point or in other words the density (ρ) is not constant for the fluid. Mathemat-

ically, for compressible flow

$$\rho \neq \text{constant}$$

Incompressible flow is that type of flow in which the density is constant for the fluid flow. Liquids are generally incompressible while gases are compressible. Mathematically, for incompressible flow

$$\rho = \text{constant.}" \text{ [28]}$$

2.4.4 Inviscous Flow

"A flow in which viscosity of the fluid is equal to zero is known as inviscous (inviscid) flow."[28]

2.5 Porous Material

"A solid containing holes or voids, either connected or non-connected, dispersed within it in either a regular or random manner known as porous material provided that holes occur relatively frequently within the solid."[28]

2.5.1 Permeability

"Permeability is the property of a porous material which characterizes the ease with which a fluid may be made to flow through the material by an applied pressure gradient. Permeability is the fluid conductivity of the porous material".

If horizontal linear row of an incompressible fluid is established through a sample of porous material of length L in the direction of flow, and cross sectional area A, then the permeability K of the material is defined as

$$K = \frac{q\mu}{A\left(\frac{\delta P}{L}\right)}$$

q is the fluid flow rate in volume per unit time, μ is the viscosity of the fluid and δP is the applied pressure difference across the length of the specimen.[28]

2.6 Conservation Laws

2.6.1 Law of Conservation of Energy

"The law of conservation of energy(or the first law of thermodynamics) states that the time rate of change of the total energy is equal to the sum of the rate of work done by applied forces and change of heat content per unit time.

$$\frac{\partial \rho e}{\partial t} + \nabla.\rho \mathbf{v}\ e = -\nabla.\mathbf{q} + Q + \phi,$$

where ϕ is the dissipation function."[30]

2.6.2 Newton's Law of Viscosity

"It states that the shear stress (τ) on a fluid element layer is proportional to the rate of shear strain. The constant of proportionally is called coefficient of viscosity. Mathematically, it is expressed as

$$\tau = \mu \frac{\partial u}{\partial y}."$$

2.6.3 Equation of Momentum

"The momentum equation states that the time rate of change of linear momentum of a given set of particles is equal to the vector sum of all the external forces acting on the particles of the set, provided Newton's Law of action and reaction governs the internal forces. Mathematically, it can be written as:

$$\frac{\partial}{\partial t}(\rho \mathbf{u}) + \rho u * u = \nabla.\mathbf{T} + \rho g."[31]$$

2.6.4 Law of Conservation of Mass

"The principle of conservation of mass can be stated as the time rate of change of mass in a fixed volume is equal to the net rate of ow of mass across the surface. The mathematical statement of the principle results in the following equation, known as the

continuity (of mass) equation

$$\frac{\partial \rho}{\partial t} + \delta.\left(\rho V\right), \tag{2.1}$$

where ρ is the density (kg/m^3) of the medium, V the velocity vector (ms^{-1}), and δ is the nabla or del operator. The continuity equation in (2.1) is in conservation (or divergence) form since it can be derived directly from an integral statement of mass conservation. By introducing the material derivative or Eulerian derivative operator $\frac{D}{Dt}$

$$\frac{D}{Dt} = \frac{\partial}{\partial t} + V.\delta, \tag{2.2}$$

the continuity equation (2.1) can be expressed in the alternate, non-conservation (or advective) form

$$\frac{\partial \rho}{\partial t} + V.\delta\rho + \rho\delta.V = \frac{D\rho}{Dt} + \rho\delta.V \tag{2.3}$$

For steady-state conditions the continuity equation becomes

$$\delta.\left(\rho V\right) = 0. \tag{2.4}$$

When the density changes following a fluid particle are negligible, the continuum is termed incompressible and we have $\frac{D\rho}{Dt}$. The continuity equation (2.3) the becomes

$$\delta.V = 0, \tag{2.5}$$

which is often referred to as the incompressibility condition or incompressibility constraint" [31].

2.7 Dimensionless Parameters

2.7.1 Prandtl Number

"The ratio of kinematic diffusivity to heat the diffusivity is said to be Prandtl number. It is denoted by Pr. Mathematically, it can be written as

$$\begin{aligned} Pr =& \frac{\nu}{\alpha} \\ =& \frac{\mu c_p}{\rho k} \end{aligned}$$

where μ denote the density of the fluid, α denote the momentum diffusivity or kinetic diffusivity and thermal diffusivity respectively." [30]

2.7.2 Thermophoresis Parameter

"In a temperature gradient, small particles are pushed towards the lower temperature because of the asymmetry of molecular impacts." [30]

2.7.3 Nusselt Number (Nu)

"It is the relationship between the convective to the conductive heat transfer through the boundary of the surface. Mathematically, it is defined as

$$Nu = \frac{hL}{k}$$

where h stands for convective heat transfer, L stands for characteristic length and k stands for thermal conductivity." [30]

2.7.4 Skin Friction Coefficient

"The skin friction coefficient is typically defined as

$$Cf = \frac{2\tau_w}{\rho U_w^2}$$

where τ_w is the local wall shear stress, ρ is the fluid density and U_w is the free stream velocity (usually taken outside the boundary layer or at the inlet)." [30]

2.7.5 Reynolds Number

"It is the most significant dimensionless number which is used to identify the different flow behaviors like laminar or turbulent flow. Mathematically, it is expressed as

$$Re = \frac{LU}{\nu}$$

where U denotes the free stream velocity, L is the characteristic length and ν stands for kinematic viscosity." [30]

2.8 Shooting Method

To elaborate the shooting method, take into account the subsequent nonlinear boundary value problem.

Example 1:

$$\left.\begin{aligned} F''(\eta) - F(\eta) + F^2(\eta) = 0 \\ F'(0) = 0, \quad F(b) = 0. \end{aligned}\right\} \tag{2.6}$$

To reduce the order of the above BVP, introduce the following notations:

$$F(\eta) = P_1, \quad F'(\eta) = P_1' = P_2. \tag{2.7}$$

The system of first order ODEs that results form the above conversion is as follows:

$$\left.\begin{aligned} P_1' = P_2, & \qquad P_1(0) = 0. \\ P_2' = P_1^2 - P_1, & \qquad P_2(0) = l. \end{aligned}\right\} \tag{2.8}$$

Where,u is the initial condition which will be guessed. The $RK4$ method will be used to numerically solve the above IVP. Choose missing condition l in such a way that

$$P_1(b, l) = 0. \tag{2.9}$$

The above equation can be solved by using Newton's method with the following iterative scheme:

$$l^{(m+1)} = l^{(m)} - \frac{P_1(b, l)^{(m)}}{\left(\frac{\partial P_1(b,l)}{\partial l}\right)^{(m)}}. \tag{2.10}$$

To find $\left(\frac{\partial P_1(b,l)}{\partial l}\right)^{(m)}$, introduced the following notations:

$$\frac{\partial P_1}{\partial l} = P_3, \quad \frac{\partial P_2}{\partial l} = P_4. \tag{2.11}$$

As a result of these new notations the Newton's iterative scheme, will then get the form

$$l^{(m+1)} = l^{(m)} - \frac{P_1\,(b,l)^{(m)}}{P_3\,(b,l)^{(m)}}. \tag{2.12}$$

Now differentiating the system of two first order ODEs in (2.4) with respect to l, we get another system of ODEs, as follows:

$$\left.\begin{aligned} P_3' &= P_4, & P_3(0) &= 0. \\ P_4' &= 2P_1P_3 - P_3, & P_4(0) &= 1. \end{aligned}\right\} \tag{2.13}$$

Writing ODEs (2.4) and (2.9) together, following IVP is obtained.

$$\begin{aligned} P_1' &= P_2, & P_1(0) &= 0. \\ P_2' &= P_1^2 - P_1, & P_2(0) &= l. \\ P_3' &= P_4, & P_3(0) &= 0. \\ P_4' &= 2P_1P_3 - P_3, & P_4(0) &= 1. \end{aligned}$$

The termination criteria for Newton's method is specified as follows.

$$|P_1(b,l)| < \epsilon,$$

where $\epsilon > 0$ is an arbitrary small positive number.

Example 2: Consider the following linear boundary value problem (BVP):

$$\begin{aligned} &y''(\eta) - 2y'(\eta) + y(\eta) = 0, \\ &y(0) = 1, \\ &y(1) = 2. \end{aligned} \tag{2.14}$$

Step 01: Convert to First-Order System

Define:

$$\begin{aligned} P_1(\eta) &= y(\eta), \\ P_2(\eta) &= y'(\eta). \end{aligned} \tag{2.15}$$

The second-order ODE can be converted into a system of first-order ODEs:

$$\begin{aligned} P_1'(\eta) &= P_2(\eta), \\ P_2'(\eta) &= 2P_2(\eta) - P_1(\eta). \end{aligned} \tag{2.16}$$

Step 02: Assign missing initial condition

With initial conditions:

$$\begin{aligned} P_1(0) &= 1, \\ P_2(0) &= U. \end{aligned} \tag{2.17}$$

Where U is the missing initial condition. We need to find U such that:

$$P_1(U) = 2. \tag{2.18}$$

Step 02: Implement the RK4 Method

After assigning missing initial condition. To solve the initial value problem (IVP) numerically, use the Runge-Kutta 4th-order (RK4) method for the system:

$$\begin{aligned} P_1'(\eta) &= P_2(\eta), \\ P_2'(\eta) &= 2P_2(\eta) - P_1(\eta). \end{aligned} \tag{2.19}$$

Step 03: Check convergence

The termination criterion for Newton's method is:

$$|P_1(1, U) - 2| < \epsilon, \tag{2.20}$$

where $\epsilon > 0$ is a small positive number.

Step 03: Apply Newton's Method

Define the function $g(U)$ as:

$$g(U) = P_1(1, U) - 2, \tag{2.21}$$

where $P_1(1, U)$ is the value of P_1 at $\eta = 1$ with the shooting parameter U.

Use Newton's method to iteratively update U:

$$U^{(m+1)} = U^{(m)} - \frac{g(l^{(m)})}{g'(U^{(m)})}. \tag{2.22}$$

To compute $g'(U)$, differentiate the system with respect to l. Introduce:

$$\frac{\partial P_1}{\partial U} = P_3, \quad \frac{\partial P_2}{\partial U} = P_4. \tag{2.23}$$

The sensitivity system is:

$$\begin{aligned} P_3'(\eta) &= P_4(\eta), \\ P_4'(\eta) &= 2P_4(\eta) - P_3(\eta), \end{aligned} \tag{2.24}$$

with initial conditions:

$$\begin{aligned} P_3(0) &= 0, \\ P_4(0) &= 1. \end{aligned} \tag{2.25}$$

Combine the original system and the sensitivity system to form a complete IVP:

$$\begin{aligned} P_1'(\eta) &= P_2(\eta), \\ P_2'(\eta) &= 2P_2(\eta) - P_1(\eta), \\ P_3'(\eta) &= P_4(\eta), \\ P_4'(\eta) &= 2P_1(\eta)P_3(\eta) - P_3(\eta). \end{aligned} \tag{2.26}$$

Repeated these step untill we get the required convergence.

Chapter 3

Scrutinization of MHD Stagnation Point Flow in Hybrid NanoFluid

3.1 Introduction

The primary focus of this chapter is to conduct a numerical investigation of the time-dependent flow behavior of a hybrid nanofluid consisting of $Al_2O_3 - Cu/H_2O$ near a stagnant point over a stretched permeable sheet, considering the influences of thermal radiation and magnetic field. The computational model for this analysis was proposed and executed by Bushra et al. [32] using the shooting method in conjunction with the fourth-order Runge-Kutta method. Transforming the governing nonlinear partial differential equations into a set of dimensionless ordinary differential equations is a prerequisite for applying the shooting method. In summary, the results of the numerical computations for various parameters, focusing on the dimensionless velocity f', temperature distribution θ, and concentration distribution ϕ, are discussed and visualized through tables and graphs.

3.2 Physical Model

Consider a scenario involving the two-dimensional unsteady flow of a hybrid nanofluid passing through a permeable sheet undergoing stretching or shrinking. The flow direction aligns with the r-axis, while the z-axis is orthogonal to the sheet. Fig.3.1 provides a visual depiction of the problem's geometry using cylindrical polar coordinates. At $z = 0$ there is a radiative permeable sheet capable of stretching or shrinking. Both the free stream temperature T_∞ and the sheet temperature T_w remain constant, while a variable magnetic field B operates perpendicular to the sheet's axis.

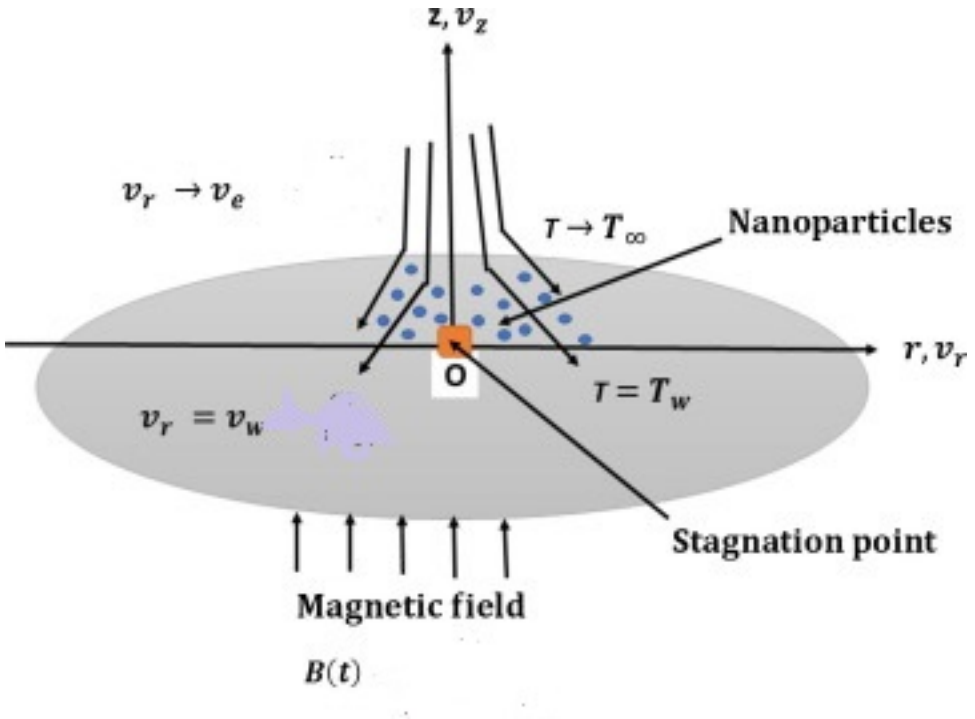

FIGURE 3.1: Flow Pattern Illustration.

Mass conservation equation:

$$\frac{\partial v_r}{\partial r} + \frac{v_r}{r} + \frac{\partial v_z}{\partial z} = 0. \tag{3.1}$$

Momentum equation:

$$\frac{\partial v_r}{\partial t} + v_r\frac{\partial v_r}{\partial r} + v_z\frac{\partial v_r}{\partial z} - \frac{\partial v_e}{\partial t} - v_e\frac{\partial v_e}{\partial r} = \frac{\mu_{hnf}}{\rho_{hnf}}\frac{\partial^2 v_r}{\partial z^2}\frac{\sigma_{hnf}B^2(t)}{\rho_{hnf}}(v_r - v_e). \tag{3.2}$$

Energy equation:

$$\frac{\partial T}{\partial t}+v_r\frac{\partial T}{\partial r}+v_z\frac{\partial T}{\partial z}=\frac{k_{hnf}}{(\rho c_p)_{hnf}}\frac{\partial^2 T}{\partial z^2}-\frac{1}{(\rho c_p)_{hnf}}\frac{\partial q_r}{\partial z}. \tag{3.3}$$

Boundary conditions:

$$\left.\begin{aligned} &v_r(r,t)=v_w(r,t)=\frac{ar}{1-et}, \quad v_z=v_0, \quad T=T_w, \quad at\ z=0,\\ &v_r(r,t)\to v_e(r,t)=\frac{br}{1-et}, \quad T\to T_\infty, \quad as\ z\to\infty. \end{aligned}\right\} \tag{3.4}$$

3.3 Similarity Transformation and Non- Dimensionalization of Mathematical Model

In this section, we present the process of non-dimensionalization for the mathematical model governing the behavior of our hybrid nanofluid. The procedure requires introducing the dimensionless variables and parameters to transform the original equations into a simpler form. By using dimensionless quantities, we gain a deeper insight into the physical phenomena and make the analysis more tractable. The mathematical model will be transformed into a system of ODEs using the following similarity transformation:

$$\left.\begin{aligned} &v_r=-\frac{1}{r}\frac{\partial\psi}{\partial z}\ , \quad v_z=\frac{1}{r}\frac{\partial\psi}{\partial r}.\\ &\eta=\frac{z}{r}Re^{\frac{1}{2}}, \quad Re=\frac{v_e r}{\nu}, \quad \theta(\eta)=\frac{T-T_\infty}{T_w-T_\infty}, \quad \psi=-\frac{v_e r^2}{Re^{\frac{1}{2}}}f(\eta), \quad v_e=\frac{br}{1-et}. \end{aligned}\right\} \tag{3.5}$$

To have the dimensionless form of the above model, The following derivatives are required to satisfy the mass conservation equation (3.1).

- $$\begin{aligned} v_r&=-\frac{1}{r}\frac{\partial\psi}{\partial z}.\\ &=-\frac{1}{r}\frac{\partial}{\partial z}\left(-\frac{v_e r^2}{Re^{\frac{1}{2}}}f(\eta)\right).\\ &=\frac{1}{r}\frac{v_e r^2}{Re^{\frac{1}{2}}}\frac{\partial}{\partial z}f(\eta).\\ &=\frac{v_e r^2}{Re^{\frac{1}{2}}}f'(\eta)\frac{\partial\eta}{\partial z}.\\ &=\frac{1}{r}\frac{v_e r^2}{Re^{\frac{1}{2}}}f'(\eta)\frac{\partial\eta}{\partial z}.\\ &=v_e f'(\eta). \end{aligned}$$

- $\dfrac{\partial v_r}{\partial r} = \dfrac{\partial}{\partial r} v_e f'(\eta).$
$= \dfrac{\partial}{\partial r} \dfrac{br}{1-et} f'(\eta).$
$= \dfrac{b}{1-et} f'(\eta).$
- $\psi = -\dfrac{v_e r^2}{Re^{\frac{1}{2}}} f(\eta).$
$= -\dfrac{br}{1-et} r^2 \sqrt{\dfrac{\nu}{v_e r}} f(\eta).$
$= -v_e r^2 \sqrt{\nu} \dfrac{1}{\sqrt{v_e r}} f(\eta).$
$= -\sqrt{\dfrac{br}{1-et} r^3}\ f(\eta)\sqrt{\nu}.$
$= -r^2 \sqrt{\dfrac{b}{(1-et)}}\ f(\eta)\sqrt{\nu}.$
$= -2r \sqrt{\dfrac{b\nu}{(1-et)}}\ f(\eta).$
- $\dfrac{\partial \psi}{\partial r} = -2\sqrt{\dfrac{b\nu}{1-et}}\ r f(\eta).$
- $\eta = \dfrac{z}{r}\sqrt{\dfrac{v_e r}{\nu}}.$
$= \dfrac{z}{r}\sqrt{\dfrac{br\ r}{(1-et)\nu}}.$
$= \dfrac{z}{r}\sqrt{\dfrac{br^2}{(1-et)\nu}}.$
$= z\sqrt{\dfrac{b}{(1-et)\nu}}.$
- $\dfrac{\partial \eta}{\partial z} = \sqrt{\dfrac{b}{(1-et)\nu}}.$
- $v_z = \dfrac{1}{r}\dfrac{\partial \psi}{\partial r}.$
$= -2\dfrac{1}{r}\sqrt{\dfrac{b\nu}{1-et}}\ r f(\eta).$
$= -2\sqrt{\dfrac{b\nu}{1-et}}\ f(\eta).$
$= -2\sqrt{\dfrac{b\nu\ r}{(1-et)r}}\ f(\eta).$
$= -2\sqrt{\dfrac{br}{(1-et)}}\sqrt{\dfrac{\nu}{r}}\ f(\eta).$
$= -2\sqrt{v}_e \sqrt{\dfrac{\nu}{r}}\sqrt{\dfrac{v_e}{v_e}}\ f(\eta).$
$= -2\sqrt{v}_e \sqrt{\dfrac{\nu}{r v_e}}\sqrt{v_e}\ f(\eta).$

$$= -2v_e Re^{-\frac{1}{2}} f(\eta).$$
$$= -2\sqrt{\frac{br}{1-et}}\ f(\eta)\sqrt{\frac{(1-et)\nu}{\sqrt{b}r}}.$$
$$= -2\sqrt{\frac{b\nu}{1-et}}\ f(\eta).$$

- $\frac{\partial v_z}{\partial z} = -2\sqrt{\frac{b\nu}{1-et}}\ f'(\eta)\frac{\partial \eta}{\partial z}.$
$$= -2\sqrt{\frac{b\nu}{1-et}}\ f'(\eta)\sqrt{\frac{b}{(1-et)\nu}}\ .$$
$$= -2\frac{b}{1-et}\ f'(\eta).$$

Now,we substitude the above partial derivatives into the (3.1)

$$\frac{b}{1-et}f'(\eta)\ + \frac{b}{1-et}f'(\eta) - 2\frac{b}{1-et}\ f'(\eta) = 0.$$

Hance equation (3.1) is identically satisfied.

TABLE 3.1: Thermo-physical properties of water base fluid and nanoparticles.

Nanofluid	**Hybrid Nanofluid**
$\rho_{nf} = \rho_f(1-\phi) + \phi\left(\frac{\rho_s}{\rho_f}\right)$	$\rho_{hnf} = \rho_f(1-\phi_{Cu})\left((1-\phi_{Al}) + \phi_{Al}(\frac{\rho_{Al}}{\rho_f})\right) + \phi_{Cu}\rho_{Cu}$
$\mu_{nf} = \frac{\mu_f}{(1-\phi)^{2.5}}$	$\mu_{hnf} = \frac{\mu_f}{(1-\phi_{Al})^{2.5}(1-\phi_{Cu})^{2.5}}$
$\frac{K_{nf}}{K_f} = \frac{K_s+(s-1)K_f-\phi(s-1)(K_f-K_s)}{K_s+(s-1)K_f+\phi(K_f-K_s)}$	$\frac{K_{hnf}}{K_{bf}} = \frac{K_{Cu}+(s-1)K_f-(s-1)\phi_{Al}(K_{bf}-K_f)}{K_{Cu}+(s-1)K_{bf}+\phi_{Al}(K_{bf}-K_{Al})}$
$(\rho c_p)_{nf} = (\rho c_p)_f\left(1-\phi+\phi\frac{(\rho c_p)_s}{(\rho c_p)_f}\right)$	$\frac{(\rho c_p)_{hnf}}{(\rho c_p)_f} = (1-\phi_{Cu})\left((1-\phi_{Al}) - \phi_{Al}\frac{(\rho c_p)_{Al}}{(\rho c_p)_f}\right) + \phi_{Cu}\frac{(\rho c_p)_{Cu}}{(\rho c_p)_f}$
	$\frac{K_{nf}}{K_f} = \frac{K_s+(s-1)K_f-(s-1)\phi(K_f-K_s)}{K_s+(s-1)K_f+\phi(K_f-K_s)}$
$\sigma_{nf} = \sigma_f\left[1+\frac{3(\sigma-1)\phi}{(\sigma+2)-(\sigma-1)\phi}\right]$	$\sigma_{hnf} = \sigma_{bf}\left[\frac{\sigma_{Cu}+2\sigma_{bf}-2\phi_{Cu}\left(\sigma_{bf}-\sigma_{Cu}\right)}{\sigma_{Cu}+2\sigma_{bf}+\phi_{Al}\left(\sigma_f-\sigma_{Cu}\right)}\right]$
	with $\sigma_{bf} = \sigma_f\left[\frac{\sigma_{Al}+2\sigma_f-2\phi_{Al}\left(\sigma_f-\sigma_{Al}\right)}{\sigma_{Al}+2\sigma_f+\phi_{Al}\left(\sigma_f-\sigma_{Al}\right)}\right]$

3.3.1 Non-Dimensionalization of Momentum Equation

For the momentum equation (3.2), the following derivatives are needed:

- $\frac{\partial v_r}{\partial t} = br\frac{\partial}{\partial t}\left(\frac{f'(\eta)}{1-et}\right).$
  $= \frac{br}{(1-et)^2}\left[1 - et\frac{\partial}{\partial t}f'(\eta) - f'(\eta)\frac{\partial}{\partial t}(1-et)\right].$
  $= \frac{br}{(1-et)^2}\left[(1-et)f''(\eta)\frac{\partial \eta}{\partial t} - f'(\eta)\ (-e)\right]$
  $= \frac{br}{(1-et)^2}\left[(1-et)f''(\eta)\frac{e\eta}{2(1-et)} \ + \ ef'(\eta)\right].$
  $= \frac{ebr\eta}{2(1-et)^2}\ f''(\eta) \ + \ \frac{ber}{(1-et)^2}f'(\eta).$
- $\frac{\partial \eta}{\partial t} = z\sqrt{\frac{b}{\nu}}\frac{\partial}{\partial t}\left[\frac{1}{(1-et)^{\frac{1}{2}}}\right].$
  $= -\frac{z}{2}\sqrt{\frac{b}{\nu}}(1-et)^{-\frac{1}{2}-1}\ (-e) = \frac{ze}{2}\sqrt{\frac{b}{\nu}}\ (1-et)^{-\frac{1}{2}-1}.$
  $= \frac{e\eta}{2(1-et)}.$
- $\frac{\partial v_r}{\partial r} = \frac{\partial}{\partial r}\left[\frac{br}{1-et}f'(\eta)\right] = \frac{b}{1-et}f'(\eta).$
  $= \frac{\partial}{\partial z}\left[\frac{br}{1-et}f'(\eta)\right] = \frac{br}{1-et}\frac{\partial}{\partial z}\left(f'(\eta)\right) = \frac{br}{1-et}f''(\eta)\frac{\partial \eta}{\partial z} = \frac{b^{\frac{3}{2}}r}{\nu^{\frac{1}{2}}(1-et)^{\frac{3}{2}}}\ f''(\eta).$
- $\frac{\partial^2 v_r}{\partial z^2} = \frac{\partial}{\partial z}\left[\frac{b^{\frac{3}{2}}r}{\nu^{\frac{1}{2}}(1-et)^{\frac{3}{2}}}f''(\eta)\right] = \frac{b^{\frac{3}{2}}r}{\nu^{\frac{1}{2}}(1-et)^{\frac{3}{2}}}\frac{\partial}{\partial z}f''(\eta) = \frac{b^{\frac{3}{2}}r}{\nu^{\frac{1}{2}}(1-et)^{\frac{3}{2}}}f'''(\eta)\frac{\partial \eta}{\partial z}.$
  $= \frac{b^{\frac{3}{2}}r}{\nu^{\frac{1}{2}}(1-et)^{\frac{3}{2}}}\sqrt{\frac{b}{\nu(1-et)}}f'''(\eta).\frac{\partial^2 v_r}{\partial z^2} = \frac{b^2 r}{\nu(1-et)}\ f'''(\eta).$
- $\frac{\partial v_e}{\partial r} = \frac{\partial}{\partial r}\left[\frac{br}{1-et}\right] = \frac{b}{1-et}.$
- $\frac{\partial v_e}{\partial t} = \frac{\partial}{\partial t}\left[\frac{br}{1-et}\right] = -br\frac{\partial}{\partial t}(1-et)^{-1} = \ -br(1-et^{-2})(-e) = \frac{ber}{(1-et)^2}.$

Now,we substitude the above partial derivatives into the (3.2) to get the following.

$$\frac{ebr\eta}{2(1-et)^2}\ f''(\eta) + \frac{ber}{(1-et)^2}f'(\eta) + \left(\frac{br}{1-et}f'(\eta)\right)\left(\frac{b}{1-et}f'(\eta)\right)$$
$$- \left(2\sqrt{\frac{b\nu}{1-et}}f\right)\left(\frac{b^{\frac{3}{2}}r}{\nu^{\frac{1}{2}}(1-et)^{\frac{3}{2}}}\ f''(\eta)\right) - \frac{ber}{(1-et)^2} - \frac{b^2 r}{(1-et)^2}$$
$$= \frac{\mu_{hnf}}{\rho_{hnf}}\left(\frac{b^2 r}{\nu(1-et)^2}f'''(\eta)\right) - \frac{\sigma_{hnf}}{\rho_{hnf}}\left(\frac{b_o}{(1-et)^{\frac{1}{2}}}\right)^2\left(\frac{br}{1-et}f'(\eta) - \frac{br}{1-et}\right).$$

$$\Rightarrow \frac{ebr\eta}{2(1-et)^2} f''(\eta) + \frac{ber}{(1-et)^2} f'(\eta) + \frac{b^2r}{(1-et)^2}(f'(\eta))^2 - \frac{2b^2r}{(1-et)^2} f(\eta)f''(\eta)$$
$$- \frac{ber}{(1-et)^2} - \frac{b^2r}{(1-et)^2}$$
$$= \frac{\mu_{hnf}}{\rho_{hnf}}\left(\frac{b^2r}{\nu(1-et)^2} f'''(\eta)\right) - \frac{\sigma_{hnf}}{\rho_{hnf}}\left(\frac{b_o^2 br}{(1-et)^2}\right)^2 \left(f'(\eta) - 1\right).$$
$$\Rightarrow \frac{e\eta}{2b} f''(\eta) + \frac{e}{b} f'(\eta) + f'(\eta)^2 - 2f(\eta)f''(\eta) - \frac{e}{b} - 1 = \frac{\mu_{hnf}}{\rho_{hnf}(\nu)} f'''(\eta)$$
$$+ \frac{\sigma_{hnf}}{\rho_{hnf}}\left(\frac{B_0^2}{b}\right)\left(1 - f'(\eta)\right).$$
$$\Rightarrow \frac{\beta\eta}{2} f''(\eta) + \beta f'(\eta) + (f'(\eta))^2 - 2f(\eta)f''(\eta) - \beta - 1 = \frac{\frac{\mu_{hnf}}{\mu_f}}{\frac{\rho_{hnf}}{\rho_f}} f'''(\eta) + M(1 - f'(\eta)).$$
$$\Rightarrow \beta\left(\frac{\eta}{2} f''(\eta) + f'(\eta) - 1\right) + f'(\eta)^2 - 2f(\eta)(f''(\eta) - 1) = \frac{\frac{\mu_{hnf}}{\mu_f}}{\frac{\rho_{hnf}}{\rho_f}} f'''(\eta) + M(1 - f'(\eta)).$$
$$\Rightarrow \frac{\frac{\mu_{hnf}}{\mu_f}}{\frac{\rho_{hnf}}{\rho_f}} f'''(\eta) + M(1 - f'(\eta)) - f'(\eta)^2 - \beta(f'(\eta) + \frac{\eta}{2} f''(\eta) - 1) + 1 + 2f(\eta)f''(\eta) = 0.$$

The dimensionless parameters are used:

$$\beta = \frac{e}{b}, \quad M = \frac{\sigma}{\frac{\rho}{b}} B_0^2.$$

3.3.2 Non-dimensionalization of Energy Equation

In this section, we discuss the non-dimensionalization process of the energy equation (3.3) for our hybrid nanofluid model.

- $\theta(\eta) = \dfrac{T - T_\infty}{T_w - T_\infty}.$
  $T - T_\infty = (T_w - T_\infty)\theta(\eta).$
  $= T_\infty + (T_w - T_\infty)\theta(\eta).$
- $\dfrac{\partial T}{\partial t} = \dfrac{\partial}{\partial t}\left[T_\infty + (T_w - T_\infty)\theta(\eta)\right].$
  $= (T_w - T_\infty)\theta'(\eta)\dfrac{\partial \eta}{\partial t}.$
  $= (T_w - T_\infty)\theta'(\eta)\dfrac{e\eta}{2(1-et)}.$
  $= (T_w - T_\infty)\dfrac{e\eta}{2(1-et)}\theta'.$
- $\dfrac{\partial T}{\partial r} = 0.$
- $\dfrac{\partial T}{\partial z} = \dfrac{\partial}{\partial z}\left[T_\infty + (T_w - T_\infty)\theta(\eta)\right].$
  $= (T_w - T_\infty)\theta'(\eta)\dfrac{\partial \eta}{\partial z}.$
  $= (T_w - T_\infty)\theta'(\eta)\sqrt{\dfrac{b}{(1-et)\nu}}.$

- $\dfrac{\partial^2 T}{\partial z^2} = (T_w - T_\infty)\sqrt{\dfrac{b}{(1-et)\nu}}\ \theta''(\eta)\dfrac{\partial \eta}{\partial z}.$

$= (T_w - T_\infty)\sqrt{\dfrac{b}{(1-et)\nu}}\ \theta''(\eta)\sqrt{\dfrac{b}{(1-et)\nu}}.$

$= (T_w - T_\infty)\dfrac{b}{(1-et)\nu}\ \theta''(\eta).$

$T^4 = T_\infty^4 + 4T_\infty^3(T - T_\infty).$

$T^4 = T_\infty^4 + 4T_\infty^3 T - 4T_\infty^4.$

- $\dfrac{\partial T^4}{\partial z} = 4T_\infty^3 \dfrac{\partial T}{\partial z}.$
- $q_r = \dfrac{-4\sigma^*}{3k^*}\dfrac{\partial T^4}{\partial z}.$

$= \dfrac{-4\sigma^*}{3k^*}\left(4T_\infty^3 \dfrac{\partial T}{\partial z}\right).$

$= \dfrac{-16\sigma^*}{3k^*}T_\infty^3\left(\dfrac{\partial T}{\partial z}\right).$

$= \dfrac{-16\sigma^*}{3k^*}T_\infty^3\left[(T_w - T_\infty)\theta'(\eta)\sqrt{\dfrac{b}{(1-et)\nu}}\ \right].$

- $\dfrac{\partial q_r}{\partial z} = \dfrac{-16\sigma^*}{3k^*}T_\infty^3\left[(T_w - T_\infty)\sqrt{\dfrac{b}{(1-et)\nu}}\ \right]\dfrac{\partial}{\partial z}\theta'(\eta).$

$= \dfrac{-16\sigma^*}{3k^*}T_\infty^3\left[(T_w - T_\infty)\sqrt{\dfrac{b}{(1-et)\nu}}\right]\ \theta''(\eta)\dfrac{\partial \eta}{\partial z}.$

$= \dfrac{-16\sigma^*}{3k^*}T_\infty^3\left[(T_w - T_\infty)\sqrt{\dfrac{b}{(1-et)\nu}}\ \right]\theta''(\eta)\sqrt{\dfrac{b}{(1-et)\nu}}\ .$

$= \dfrac{-16\sigma^*}{3k^*}T_\infty^3(T_w - T_\infty)\dfrac{b}{(1-et)\nu}\theta''(\eta).$

Now,we substitude the above partial derivatives into the (3.3) to get the following.

$$(T_w - T_\infty)\frac{e\eta}{2(1-et)}\theta' + \left(-2\sqrt{\frac{b\nu}{1-et}}f\right)\left[(T_w - T_\infty)\theta'(\eta)\sqrt{\frac{b}{(1-et)\nu}}\theta'(\eta)\right]$$
$$= \frac{k_{hnf}/k_f}{(\rho c_p)_{hnf}}\left[(T_w - T_\infty)\frac{b}{(1-et)\nu}\ \theta''(\eta)\right]$$
$$- \frac{1}{(\rho c_p)_{hnf}}\left[-\frac{16\sigma^* T_\infty^3}{3k^*}(T_w - T_\infty)\frac{b}{(1-et)\nu}\theta''(\eta)\right].$$
$$\Rightarrow \frac{e\eta}{2(1-et)}\theta'(\eta) - 2\frac{b}{1-et}f\theta'(\eta) = \frac{k_{hnf}/k_f}{(\rho c_p)_{hnf}}\left[\frac{b}{(1-et)\nu}\ \theta''(\eta)\right].$$
$$+ \frac{1}{(\rho c_p)_{hnf}}\left[\frac{16\sigma^* T_\infty^3}{3k^*}\frac{b}{(1-et)\nu}\theta''(\eta)\right].$$
$$\Rightarrow \frac{\eta e}{2(1-et)}\theta'(\eta) - 2f\theta'(\eta) = \frac{k_{hnf}/k_f}{(\rho c_p)_{hnf}}\frac{1}{\nu}\theta'' + \frac{1}{(\rho c_p)_{hnf}\nu}\left[\frac{16\sigma^* T_\infty^3}{3k^*}\right]\theta''$$
$$\frac{k_{hnf}/k_f}{((\rho c_p)_{hnf})\frac{\mu_f}{\rho_f}}\left[1 + \frac{16\sigma^* T_\infty^3}{3k^*}\right]\theta''(\eta) + \left(2f - \frac{\eta}{2}\beta\right)\theta'(\eta) = 0.$$
$$\Rightarrow \frac{k_{hnf}/k_f}{((\rho c_p)_{hnf})\frac{\mu_f}{\rho_f}}\left[\left(1 + \frac{4}{3}Rd\right)\right]\theta''(\eta) + \left(2f - \frac{\eta}{2}\beta\right)\theta'(\eta) = 0.$$

$$\Rightarrow \frac{k_{hnf}/k_f}{(\rho c_p)_{hnf}} \frac{(\rho_f k_f)(\rho c_p)_f}{\mu_f (\rho c_p)_f} \left[\left(1+\frac{4}{3}Rd\right)\right]\theta''(\eta) + \left(2f - \frac{\eta}{2}\beta\right)\theta'(\eta) = 0.$$

$$\Rightarrow \frac{\frac{k_{hnf}}{k_f}}{Pr\frac{(\rho c_p)_{hnf}}{(\rho c_p)_f}} \left[\left(1+\frac{4}{3}Rd\right)\right]\theta'' + \left(2f - \frac{\eta}{2}\beta\right)\theta' = 0.$$

3.3.3 Non-dimensionalization of Boundary Conditions

The corresponding BCs are transformed into non-dimensional form through the following procedure.

$$v_r(r,t) = v_w(r,t) \qquad at \;\; \eta = 0.$$

$$\Rightarrow v_e f'(\eta) = \frac{ar}{1-et} \qquad at \;\; \eta = 0.$$

$$\Rightarrow \frac{br}{1-et} f'(\eta) = \frac{ar}{1-et} \qquad at \;\; \eta = 0.$$

$$\Rightarrow bf'(\eta) = a \qquad at \;\; \eta = 0.$$

$$\Rightarrow f'(\eta) = \frac{a}{b} \qquad at \;\; \eta = 0.$$

$$\Rightarrow f'(0) = \lambda$$

$$v_z = v_0 \qquad at \;\; z = 0.$$

$$\Rightarrow \; -2v_e f(\eta) R_e^{\frac{-1}{2}} = -2v_e S R_e^{\frac{-1}{2}}. \qquad at \; \eta \; = 0.$$

$$\Rightarrow f(\eta) = S \qquad at \;\; \eta = 0.$$

$$\Rightarrow f(0) = S$$

$$T = T_w \qquad at \;\; z = 0.$$

$$\Rightarrow T_\infty + (T_w - T_\infty)\theta(\eta) = T_w \qquad at \;\; \eta = 0.$$

$$\Rightarrow (T_w - T_\infty)\theta(\eta) = (T_w - T_\infty) \qquad at \;\; \eta = 0.$$

$$\Rightarrow \theta(\eta) = 1 \qquad at \;\; \eta = 0.$$

$$\Rightarrow \theta(0) = 1$$

$$v_r(r,t) \;\rightarrow\; v_e(r,t).$$

$$\Rightarrow v_e f'(\eta) \;\rightarrow \frac{br}{1-et} \qquad as \; \eta \rightarrow \infty.$$

$$\Rightarrow \frac{br}{1-et} f'(\eta) \rightarrow \frac{br}{1-et} \qquad as \; \eta \rightarrow \infty.$$

$$\Rightarrow f'(\eta) \rightarrow 1 \qquad as \; \eta \rightarrow \infty.$$

$$T \rightarrow T_\infty$$

$$\Rightarrow T_\infty + (T_w - T_\infty)\theta(\eta) \rightarrow T_\infty \qquad as \;\; \eta \rightarrow \infty.$$

$$\Rightarrow (T_w - T_\infty)\theta(\eta) \rightarrow 0 \qquad as \;\; \eta \rightarrow \infty.$$

$$\Rightarrow \theta(\eta) \rightarrow 0 \qquad as \;\; \eta \rightarrow \infty.$$

$$\Rightarrow \theta(\eta) \rightarrow 0 \qquad as \;\; \eta \rightarrow \infty.$$

3.3.4 Non-dimensionalization of Physical Quantities

The dimensionless physical quantities section of this thesis focuses on two important parameters: the skin friction and the Nusselt number.

Skin friction:

$$\bullet\ C_f = \frac{\mu_{hnf}}{\rho_f(v_e^2)}\left(\frac{\partial v_r}{\partial z}\right) = \frac{\mu_{hnf}}{\rho_f(v_e^2)}\left[v_e f''(0)\frac{R_e^{\frac{1}{2}}}{r}\right] = \frac{\mu_{hnf}}{\rho_f(v_e^2)}\frac{v_e^{\frac{3}{2}} f''(0)}{r^{\frac{1}{2}}\nu^{\frac{1}{2}}} = \frac{\mu_{hnf}}{\rho_f(v_e^2)}\frac{v_e^{\frac{3}{2}} f''(0)}{r^{\frac{1}{2}}\nu^{\frac{1}{2}}}.$$
$$= \frac{\mu_{hnf}}{\rho_f(v_e^2)}\frac{f''(0)}{r^{\frac{1}{2}}\nu^{\frac{1}{2}}} = \frac{\mu_{hnf}}{\rho_f(R_e^{\frac{1}{2}})}\frac{f''(0)}{\nu^{\frac{1}{2}}\nu^{\frac{1}{2}}} = \frac{\mu_{hnf}}{\rho_f(R_e^{\frac{1}{2}})}\frac{f''(0)}{\nu} = \frac{\mu_{hnf}}{\rho_f(R_e^{\frac{1}{2}})}f''(0).$$
$$C_f(R_e^{\frac{1}{2}}) = \frac{\mu_{hnf}}{\rho_f}f''(0).$$

Nusselt Number:

$$\bullet\ Nu = -\frac{rk_{hnf}}{k_f(T_w - T_\infty)}\frac{\partial T}{\partial z}.$$

using value of derivative

$$Nu = -\frac{rk_{hnf}}{k_f(T_w - T_\infty)}\left[(T_w - T_\infty)\theta'(\eta)\sqrt{\frac{b}{(1-et)\nu}}\right] = -r\sqrt{\frac{b}{(1-et)\nu}}\frac{k_{hnf}}{k_f}\theta'(0).$$

3.4 Solution Framework

In order to solve the ODEs of momentum equation, the shooting method has been used. The domain of the problem is to be bounded i.e [0,η_∞], where η_∞=1 real number. The following notations have been considered:

$$f = y_1, \qquad f' = y_1' = y_2, \qquad f'' = y_1'' = y_2' = y_3.$$

The momentum equations are then transformed into the following system of first-order ODEs:

$$\left.\begin{aligned} y_1' &= y_2, & y_1(0) &= S. \\ y_2' &= y_3, & y_2(0) &= \lambda. \\ y_3' &= \frac{\frac{\rho_{hnf}}{\rho_f}}{\frac{\mu_{hnf}}{\mu_f}}\left[y_2^2 - 2y_1y_3 + \beta\left(y_2 + \frac{\eta}{2}y_3 - 1\right) - 1 - M(1-y_2)\right]. & y_3(0) &= p. \end{aligned}\right\} \tag{3.6}$$

To utilize the Runge-Kutta 4th order (RK4) method for the numerical solution of the above IVP, the missing condition p within the system of equations need to be carefully chosen. The missing condition p needs to be selected so that

$$y_2(\eta_\infty, p) - 1 = 0.$$

For convenience, now onward $y_2(\eta_\infty, p)$ will be denoted by $y_2(p)$.

Let us further denote $y_2(p) - 1$ by $\phi(p)$, so that

$$\phi(p) = 0.$$

Newton's method will be used to find p. This method has the following iterative scheme:

$$p_{n+1} = p_n - \frac{\phi(p_n)}{\phi'(p_n)}.$$

We further introduce the following notations:

$$\frac{\partial y_1}{\partial p} = y_4, \qquad \frac{\partial y_2}{\partial p} = y_5, \qquad \frac{\partial y_3}{\partial p} = y_6.$$

The Newton's iterative scheme from these new notations is:

$$p_{n+1} = \frac{y_2(p_n) - 1}{y_5(p_n)}.$$

Now, differentiating system of three first order ODEs 3.6 with respect to p, we get another system of ODEs, as follows:

$$\left.\begin{aligned} y_4' &= y_5, & y_4(0) &= 0. \\ y_5' &= y_6, & y_5(0) &= 0. \\ y_6' &= \frac{\frac{\rho_{hnf}}{\rho f}}{\frac{\mu_{hnf}}{\mu_f}}\left[2y_2y_5 - 2y_4y_3 - 2y_1y_6 + \beta\left(y_5 + \frac{\eta}{2}y_6\right) + My_5\right] = 0. & y_6(0) &= 1. \end{aligned}\right\} \tag{3.7}$$

The criteria for terminating Newton's technique is defined as:

$$\left|y_2(p_n) - 1\right)\right| < \epsilon,$$

where $\epsilon > 0$ is an arbitrarily small positive number. From now onward, ϵ has been taken as 10^{-6}.

Now, to solve the energy equation numerically by using shooting method, f and f'' will be taken as known functions. The notations below are used for the implementation of the shooting method.

$$\theta = Z_1, \qquad \theta' = z_1' = Z_2, \qquad \theta'(0) = m.$$

The energy equation can be formulated as the following system of first-order coupled ODEs:

$$\left.\begin{aligned} Z_1' &= Z_2, & Z_1(0) &= 1. \\ Z_2' &= -\left(2f - \frac{\eta}{2}\beta\right)3\theta'\left[\frac{Pr(\rho C_p)_{hnf}/(\rho C_p)_f}{\frac{k_{hnf}}{k_f}(3 + 4Rd)}\right]. & Z_2(0) &= m. \end{aligned}\right\} \tag{3.8}$$

To utilize the Runge-Kutta 4th order method for numerical solution of the above-mentioned initial value problem, the condition m within the system of equations needs to be carefully chosen.

The missing condition m needs to be selected so that:

$$Z_1(\eta_\infty, m) = 0,$$

Newton's method will be used to find m with the following iterative scheme:

$$m_{(n+1)} = m_{(n)} - \frac{Z_1\big(\eta_\infty, m_n\big)}{\big(\frac{\partial}{\partial m} Z_1\big(\eta_\infty, m\big)\big)_n}.$$

We further introduce the following notations:

$$\frac{\partial Z_1}{\partial m} = Z_3, \qquad \frac{\partial Z_2}{\partial m} = Z_4.$$

As a result of these new notations, the Newton's iterative scheme gets the form:

$$m_{n+1} = m_n - \frac{Z_1(m_n)}{Z_3(m_n)}.$$

Now differentiating the system of two first order ODEs 3.8 with respect to m, we get another system of ODEs, as follows:

$$\begin{aligned} Z_3' &= Z_4, & Z_3(0) &= 0. \\ Z_4' &= -3(2f - \frac{\eta}{2}\beta) y_4 \left[\frac{\frac{Pr(\rho C_p)_{hnf}}{(\rho C_p)_f}}{\frac{k_{hnf}}{k_f}(3 + 4Rd)} \right]. & Z_4(0) &= 1. \end{aligned}$$

The termination criteria for Newton's method is specified as follows:

$$|Z_2(m_n)| < \epsilon.$$

3.5 Results Interpretation

This section aims to evaluate the physical characteristics of velocity and energy profiles concerning the variations in several significant physical constants, such as magnetic field strength (M), unsteadiness parameter (β), suction/injection parameter (S), stretching parameter (λ), radiation parameter (Rd). The evaluation is conducted by utilizing graphical representations of velocity and temperature profiles. Furthermore, by modifying the values of dimensionless parameters, the effects of these parameters on physical quantities such as skin friction and Nusselt number are examined and presented in tabular form.

The graphical representations of velocity and temperature profiles provide visual insights into the behavior of the system as the physical parameters vary. By observing the trends in these profiles, a better understanding of the system's physical characteristics can be obtained.

3.5.1 Analysis of Computational Results

Table 3.2 presents the results of the skin friction coefficient and local Nusselt number for the Al_2O_3- Cu/H_2O hybrid nanofluid, considering different inputs of M, β, S, and λ. The findings reveal that an increase in the value of M and β leads to higher absolute values of local skin friction coefficients, indicating a decrease in the fluid velocity.

TABLE 3.2: The results of the skin friction coefficient $C_f\sqrt{Re}$ for values of various M, β, S and λ parameters when $\phi_{Al} = 0.02$ and $\phi_{Cu} = 0.02$.

M	β	S	λ	ϕ_{Al}	ϕ_{Cu}	$C_f\sqrt{Re}$	I_{C_f}
0.2	0.2	0.1	0.2	0.02	0.02	1.535798	[0.4,48.6]
0.4						1.593205	[0.9 , 6.5]
0.6						1.648616	[1.4 , 8]
0.8						1.702220	[1.2 , 3.9]
	0.3					1.558127	[0.8 , 6.9]
	0.6					1.614949	[1.1 , 3.3]
	0.8					1.653637	[1.1 , 3.3]
		-0.2				1.209142	[0.8 , 2.7]
		0				1.420724	[0.8 , 5.8]
		0.2				1.656634	[0.7 ,47.9]
			0.4			1.213781	[0.4 , 20]
			0.6			0.848219	[0 , 43.7]
			0.8			0.442668	[0.1 ,43.8]

Moreover, Table 3.3 provides details on the absolute values of the Nusselt number. The results indicate that Nusselt number decreases with higher values of Rd, reflecting enhanced heat

transfer. Furthermore, it is observed that Nusselt number increases with the suction/injection parameter (S) and stretching parameter (λ).

TABLE 3.3: The results of the skin friction coefficient $Re^{-\frac{1}{2}}Nu$ for differnt values of M, β, S, λ and Rd parameters when $\phi_{Al} = 0.02$ and $\phi_{Cu} = 0.02$.

M	β	S	λ	Rd	ϕ_{Al}	ϕ_{Cu}	$Re^{-\frac{1}{2}}Nu$
0.2	0.2	0.1	0.2	1.2	0.02	0.02	1.576334
0.4							1.583443
0.6							1.590123
0.8							1.596422
	0.3						1.549740
	0.6						1.467327
	0.8						1.409987
		-0.2					0.736723
		0					1.264331
		0.2					1.914584
			0.4				1.723083
			0.6				1.859855
			0.8				1.866753
				0.5			2.002277
				0.7			1.846952
				1.2			1.846952

3.5.2 Velocity Profile

Figures 3.2 to 3.5 provide insights into the nature of the velocity profile, denoted as $f'(\eta)$, with respect to various physical parameters. Specifically, Figure 3.2 and 3.3 illustrate the effects of the magnetic force M and unsteadiness parameter (β) on the dimensionless velocity $f'(\eta)$. It is evident that both of the nanofluids, namely Al_2O_3/H_2O and Al_2O_3-Cu/H_2O, experience a significant decrease in flow velocity as the values of these two parameters M and β increase.

Variation in the magnetic field parameter M results in a noticeable decline in the flow velocity across the fluid domain, indicating the influence of the applied magnetic field. This phenomenon is associated with the generation of the Lorentz force, resembling a drag force, within electrically conductive fluids. Similarly, increasing the unsteady parameter β results in a decrease in the velocity profiles, along with a reduction in the momentum boundary layer thickness in both scenarios. This indicates that the unsteadiness parameter diminishes the flow rate associated with the stretching sheet.

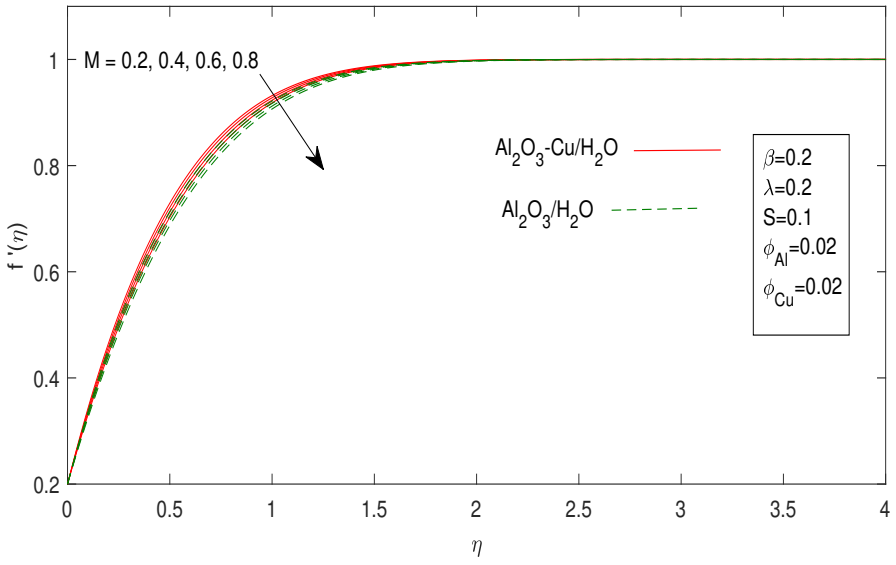

FIGURE 3.2: Influence of M on velocity profile $f'(\eta)$

Figures 3.4 and 3.5 illustrate significant findings regarding the impact of the suction/injection parameter (S) and stretching parameter (λ) on the velocity profile $f'(\eta)$. The analysis reveals that variations in both S and λ result in a reduction in fluid velocity. It's noticeable that as the suction parameter $S > 0$ rises, there is a significant decrease in velocity, whereas fluid velocity increases with injection $S < 0$. Likewise, the velocity

increases with the increasing stretching parameter λ. In conclusion, a higher stretching parameter increases the compression rate of the fluid, resulting a decline in fluid velocity.

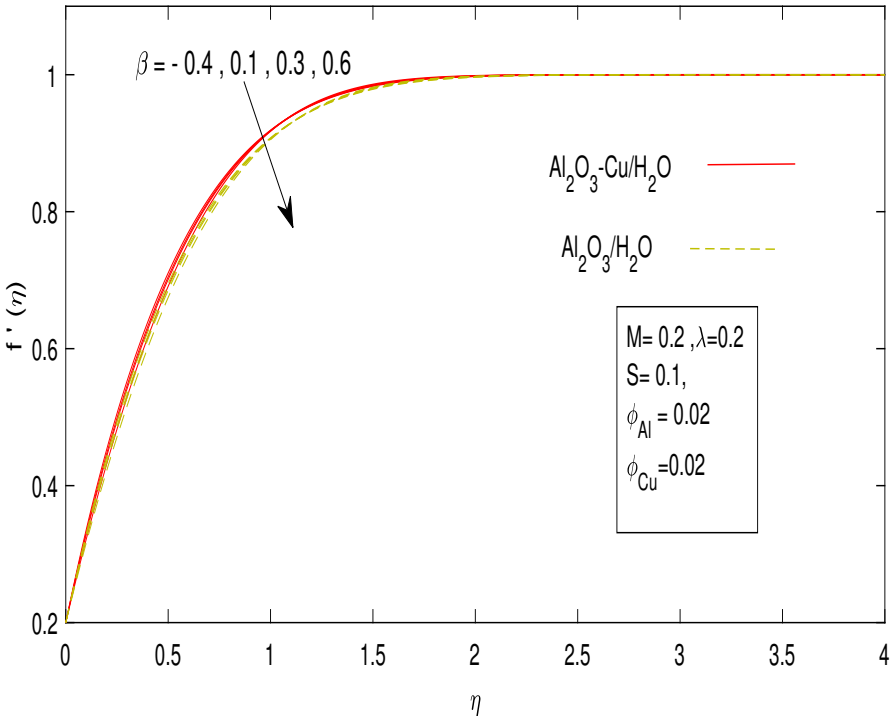

FIGURE 3.3: Influence of β on velocity profile $f'(\eta)$

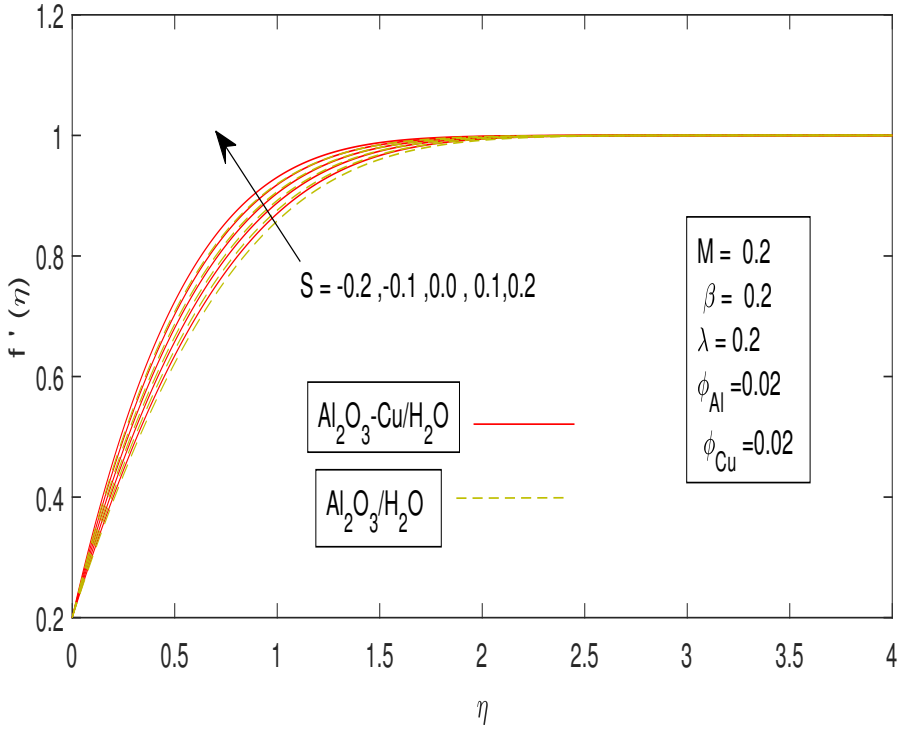

FIGURE 3.4: Influence of S on velocity profile $f'(\eta)$

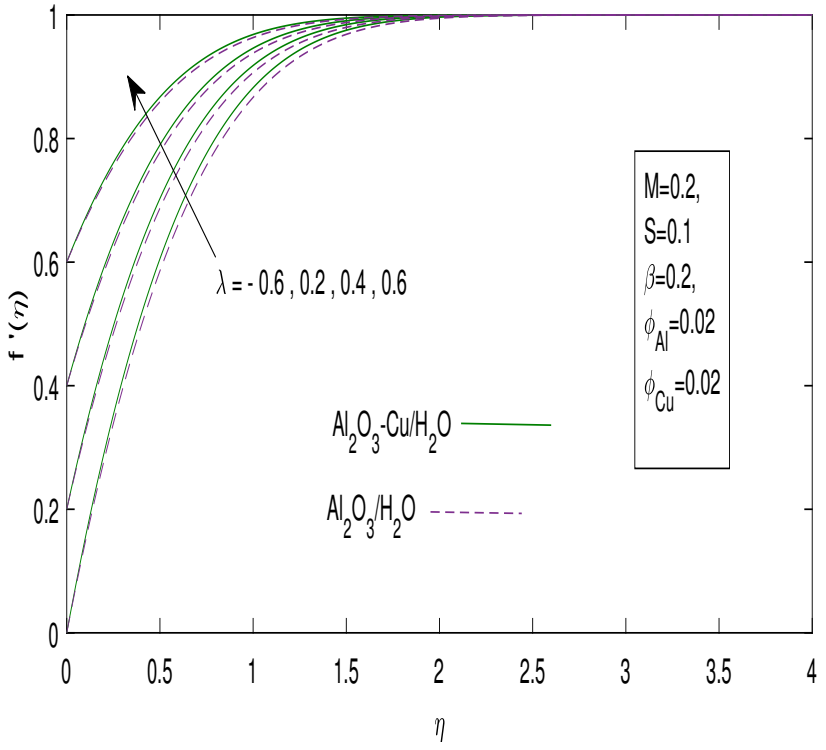

FIGURE 3.5: Influence of λ on velocity profile $f'(\eta)$

3.5.3 Temperature Profile

Figures 3.6 to 3.10 present the characteristics of the energy profile $\theta(\eta)$ with respect to various parameters, including the magnetic parameter (M), unsteadiness parameter (β), suction/injection parameter (S), stretching parameter (λ), and Radiation parameter (Rd). Figure 3.6 and 3.7 illustrate the temperature fluctuations of the fluid (both nano- and hybrid nanofluids) with varying values of M and β. It is observed that as the magnetic parameter increases, the temperature profiles demonstrate a corresponding increase. This implies that an elevation in the magnetic parameter leads to an increase in the temperature within the boundary layer. It is observed that as the values of the unsteadiness parameter increase, the temperature profile also increases. This indicates that the effect of the unsteadiness parameter causes a rise in the thermal boundary layer thickness.

Figures 3.8 and 3.9 depict the relationship between the temperature of the fluid and the suction/injection parameter (S) and stretching parameter (λ). Observations indicate that increasing the suction values ($S > 0$) lead to a decrease in the fluid temperature, while increasing injection values ($S < 0$) cause an increase. This is because suction

brings ambient fluid closer to the surface, thinning the thermal boundary layer, while injection has the opposite effect, thickening the boundary layer. While an increase in the stretching parameter results in a drop in the temperature profile. This effect is due to the increased velocity of the nanofluid from stretching, which expands the thermal boundary layer and leads to greater temperature gradients on the surface.

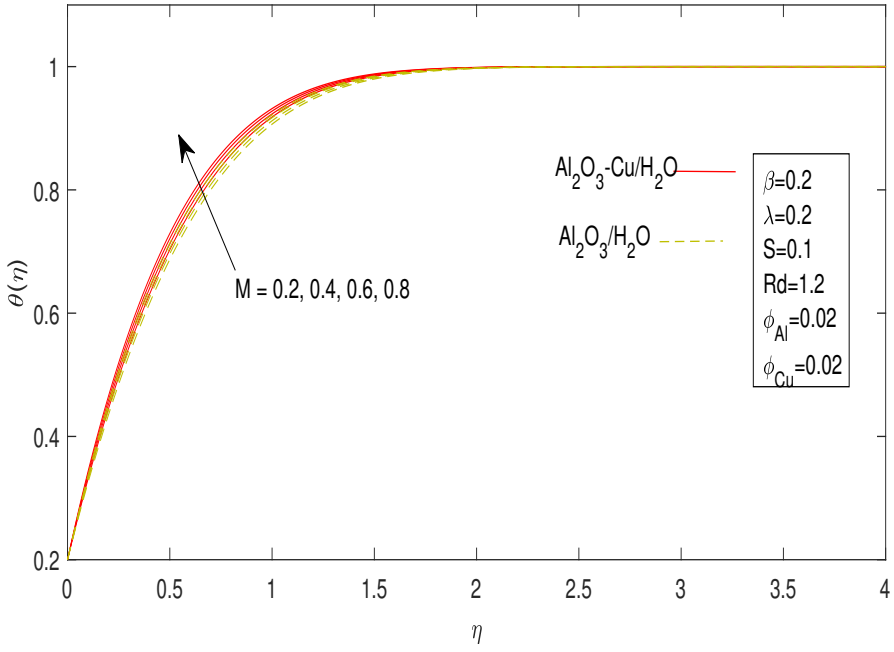

FIGURE 3.6: Influence of M on temperature profile $\theta(\eta)$

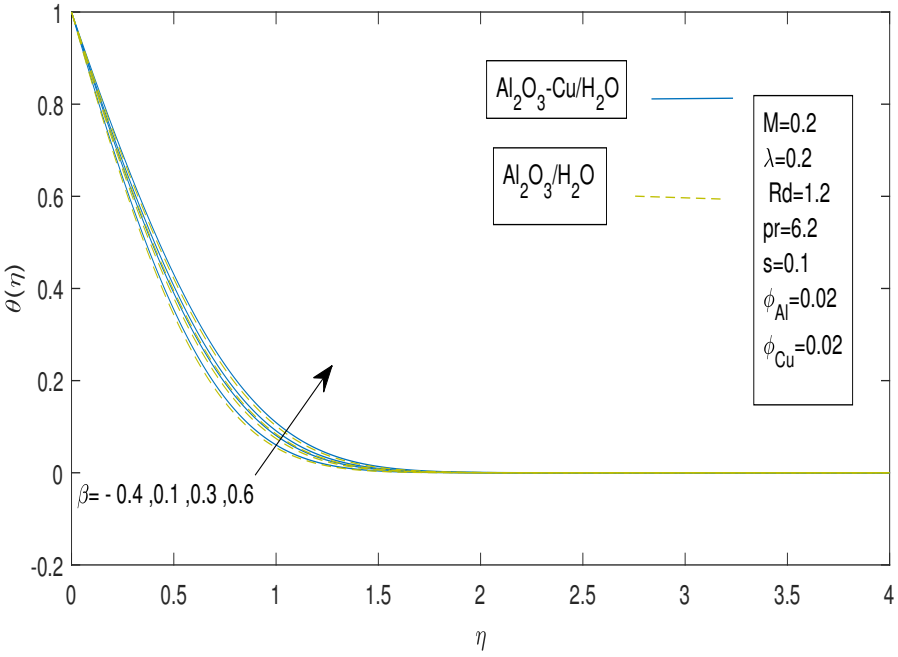

FIGURE 3.7: Influence of β on temperature profile $\theta(\eta)$

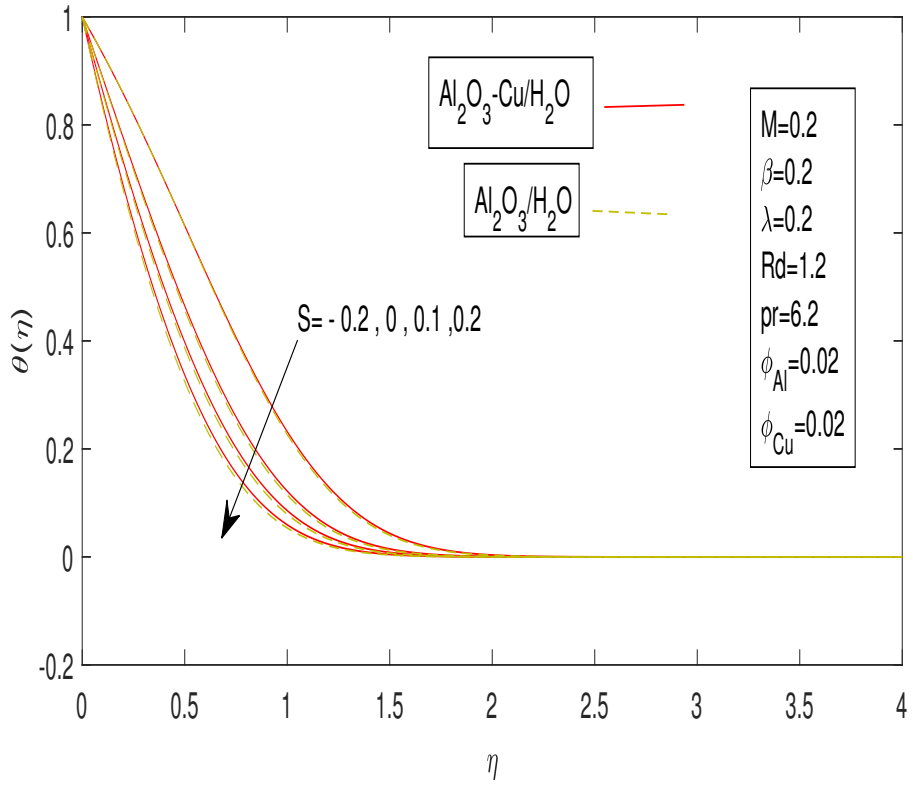

FIGURE 3.8: Influence of S on temperature profile $\theta(\eta)$

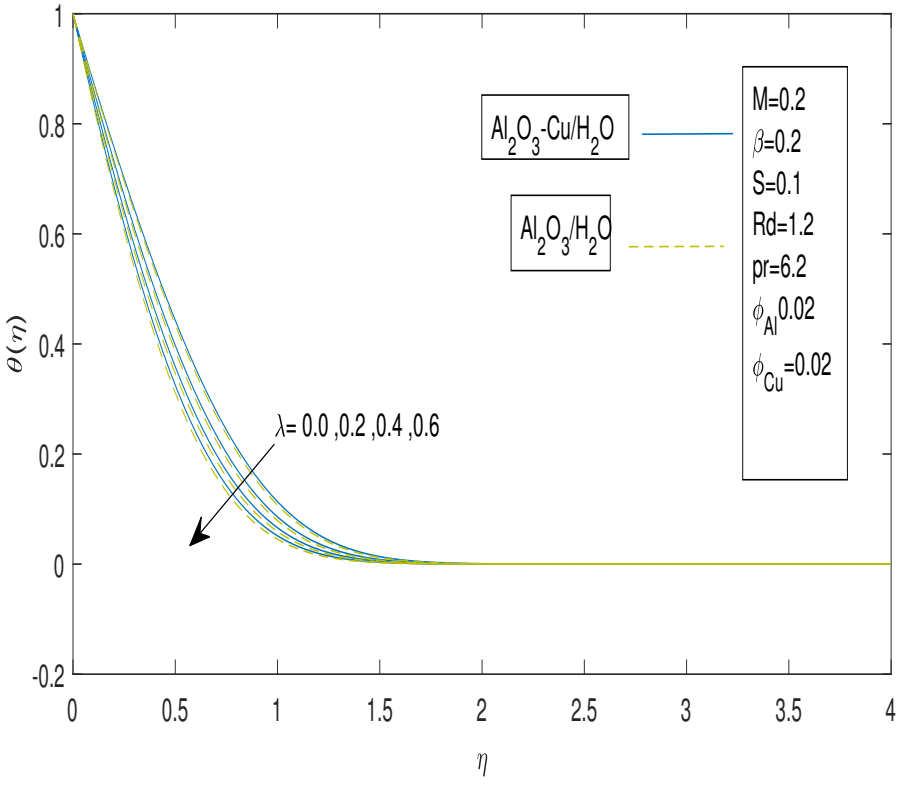

FIGURE 3.9: Influence of λ on temperature profile $\theta(\eta)$

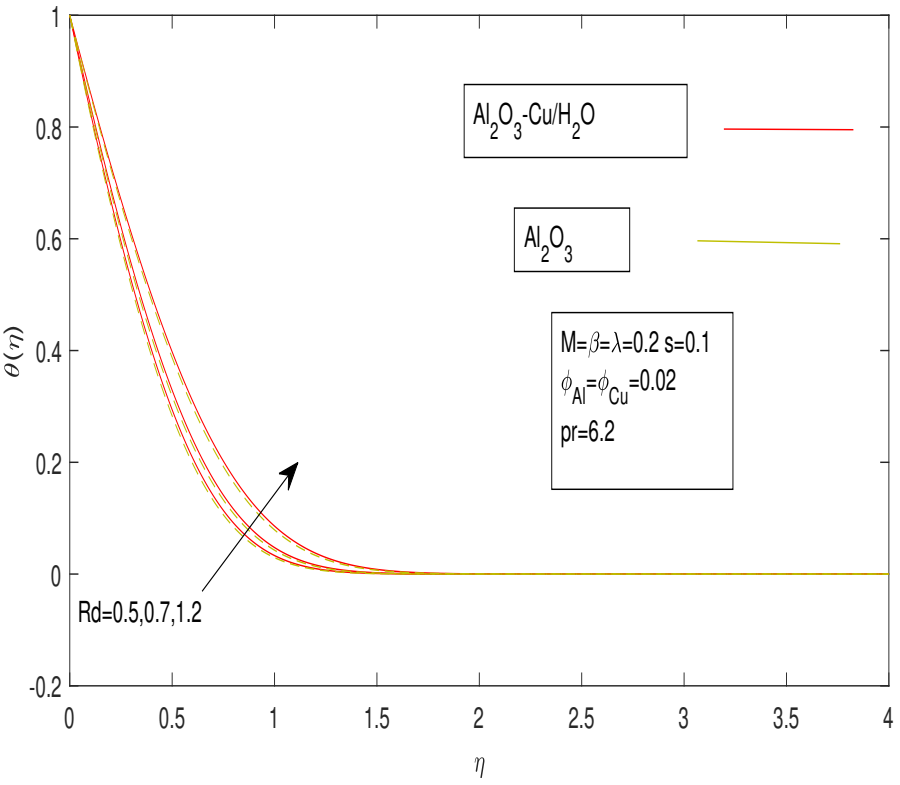

FIGURE 3.10: Influence of Rd on temperature profile $\theta(\eta)$

Chapter 4

The Influence of Cattaneo-Christov Heat Flux Model and Activation Energy on Hybrid Nanofluid Flow

4.1 Introduction

In this chapter, the magnetohydrodynamic stagnation point flow in a hybrid nanofluid model, initially discussed in Chapter 3 [32], has been modified by incorporating the Cattaneo-Christov heat flux model and the heat source effect into the energy equation, along with additional concentration equations for the water-based hybrid nanofluid ($Al_2O_3 + Cu$). This inclusion allows the examination of the combined effects of these factors on the fluid flow over a stretchable/shrinking permeable sheet. Comprehensive numerical simulations and analyses were conducted to investigate the intricate interplay of these effects and their overall impact on flow behavior. The findings from this study provide valuable insights into the behavior of the hybrid nanofluid under various physical conditions, enhancing our understanding of fluid flow in such scenarios.

4.2 Mathematical Modeling

This study investigates the flow characteristics of a hybrid nanofluid over a stretching/shrinking permeable sheet, considering a two-dimensional and unsteady boundary layer flow. The coordinate axis along the stretched sheet is denoted by r, and the axis perpendicular to the sheet is denoted by z, as shown in Figure 3.1. To analyze mass diffusion and heat transfer, the interaction of the applied magnetic field with dynamic thermal radiation and activation energy is utilized. The flow phenomenon is studied under several key assumptions, including Brownian diffusion, thermophoretic diffusion, Cattaneo-Christov heat flux, heat generation/absorption, and heat source, with a surface velocity of $v_w(x) = \frac{ax}{1-et}$ ($a > 0$, a constant). A variable magnetic field $B(t) = \frac{B_0}{(1-et)^{1/2}}$ is applied perpendicular to the sheet's axis. The temperature and concentration near the surface are T_w and C_f, respectively, while the free stream temperature and concentration of the hybrid nanofluid are T_∞ and C_∞, respectively.

Mass conservation:

$$\frac{\partial v_r}{\partial r} + \frac{v_r}{r} + \frac{\partial v_z}{\partial z} = 0. \tag{4.1}$$

Momentum Equation:

$$\frac{\partial v_r}{\partial t} + v_r\frac{\partial v_r}{\partial r} + v_z\frac{\partial v_r}{\partial z} - \frac{\partial v_e}{\partial t} - v_e\frac{\partial v_e}{\partial r} = \frac{\mu_{hnf}}{\rho_{hnf}}\frac{\partial^2 v_r}{\partial z^2}\frac{\sigma_{hnf}B^2(t)}{\rho_{hnf}}(v_r - v_e). \tag{4.2}$$

Energy Equation:

$$\begin{aligned}&\frac{\partial T}{\partial t} + v_r\frac{\partial T}{\partial r} + v_z\frac{\partial T}{\partial z} + \beta_T\left[\frac{\partial^2 T}{\partial t^2} + 2v_r\frac{\partial^2 T}{\partial r\partial t} + 2v_z\frac{\partial^2 T}{\partial z\partial t} + \frac{\partial v_z}{\partial t}\frac{\partial T}{\partial z} + v_r\frac{\partial v_r}{\partial r}\frac{\partial t}{\partial r}\right.\\ &\left. + v_z\frac{\partial v_z}{\partial z}\frac{\partial T}{\partial z} + v_r\frac{\partial v_z}{\partial v_r}\frac{\partial T}{\partial z} + v_z\frac{\partial v_r}{\partial v_z}\frac{\partial T}{\partial r} + 2v_rv_z\frac{\partial^2 T}{\partial r\partial z} + v_r^2\frac{\partial^2 T}{\partial r^2} + v_z^2\frac{\partial^2 T}{\partial z^2}\right]\\ &= \frac{k_{hnf}}{(\rho e_p)_{hnf}}\frac{\partial^2 T}{\partial z^2} - \frac{1}{(\rho e_p)_{hnf}}\frac{\partial q_r}{\partial z}.\end{aligned} \tag{4.3}$$

Concentration Equation:

$$\frac{\partial C}{\partial t} + v_r\frac{\partial C}{\partial r} + v_z\frac{\partial C}{\partial z} = D_B\frac{\partial^2 C}{\partial z^2} + \frac{D_T}{T_\infty}\frac{\partial^2 T}{\partial z^2} - K_r^2(t)(C - C_\infty)\left(\frac{T}{T_\infty}\right)^m \exp\left(\frac{-E_a}{K_1 T}\right). \tag{4.4}$$

Boundary Conditions:

The boundary conditions corresponding to the current problem are as follows:

$$\left.\begin{aligned}&v_r(r,t) = v_w(r,t) = \frac{ar}{1-et},\ v_z = v_0,\ \ T = T_w,\ D_B\frac{\partial C}{\partial z} + \frac{D_T}{T_\infty}\frac{\partial T}{\partial z} = 0,\ \ at\ z = 0,\\ &v_r(r,t) \to v_e(r,t) = \frac{br}{1-et},\ \ T \to T_\infty,\ \ C \to C_\infty,\ \ as\ z \to \infty.\end{aligned}\right\} \tag{4.5}$$

4.2.1 Formulation and Thermo-physical Characteristics

To provide a clear comparison, the valuable thermo-physical characteristics of both the HNF and the NF are presented in Table 4.1.

TABLE 4.1: Thermo-physical characteristics related to present model.

.

Physical Properties	Al_2O_3	Cu	H_2O
$\rho\left(\frac{Kg}{m^3}\right)$	3970	8954	997.1
$c_p\left(\frac{J}{KgK}\right)$	765	383	997.1
$k\left(\frac{W}{mK}\right)$	40	400	0.613
$\sigma\left(\Omega.m\right)^{-1}$	$\times 10^{-10}$	5.96×10^7	4179
Pr	6.2		

The formulation of different thermo-physical properties for both nanofluid and hybrid nanofluid are articulated in Table 3.1.

4.3 Similarity Transformation and Non- Dimensionalization of Mathematical Model

In this section, we outline the process of non-dimensionalization for the mathematical model governing the behavior of our hybrid nanofluid. This process involves introducing the dimensionless variables and parameters to simplify the original equations. By utilizing dimensionless quantities, we enhance our understanding of the physical phenomena and manage a more meaningful analysis. The mathematical model will be converted into a system of ordinary differential equations (ODEs) through the following similarity transformation:

$$\left.\begin{aligned} &\eta = \frac{z}{r}Re^{\frac{1}{2}}, \quad Re = \frac{v_e r}{\nu}, \quad \theta(\eta) = \frac{T - T_\infty}{T_w - T_\infty}, \quad \psi = -\frac{v_e r^2}{Re^{\frac{1}{2}}} f(\eta), \quad \phi(\eta) = \frac{C - C_\infty}{C_\infty}. \\ &v_r = -\frac{1}{r}\frac{\partial \psi}{\partial z} \quad , \quad v_z = \frac{1}{r}\frac{\partial \psi}{\partial r}. \end{aligned}\right\} \tag{4.6}$$

The symbol η represents the similarity variable. The velocity components in the r and z directions are denoted by v_r and v_z, respectively, while $\theta(\eta)$ and $\phi(\eta)$ stand for the dimensionless temperature and concentration profiles. Different parameters used in the upcoming ODEs and their BCs, have been listed in Table 4.2.

TABLE 4.2: Different Dimensionless parameters used in the governing ODEs

Symbols	Name	Appearance
M	Magnetic field	$M = \frac{\sigma B_o^2}{\rho a}$
β	Unsteadiness Parameter	$\beta = \frac{e}{b}$
Pr	Prandtl Number	$Pr = \frac{\nu}{\alpha}$
E	Activation Energy Parameter	$E = \frac{E_a}{K_1 T_\infty}$
Sc	Schmidt number	$Sc = \frac{\nu}{D_B}$
Nt	Thermophoresis Parameter	$Nt = \frac{\tau D_T (T_w - T_\infty)}{\nu T_\infty}$
Nb	Brownian motion parameter	$Nb = \frac{\tau D_B C_\infty}{\nu}$
Rd	Radiation Parameter	$Rd = \frac{KK^*}{4\sigma^* T_\infty^3}$
λ	Stretching parameter	$\lambda = \frac{a}{b}$
δ_T	Thermal Relaxation parameter	$\delta_T = \beta_0 b$
θ_w	Temprature ratio parameter	$\theta_w = \frac{T_w}{T_\infty}$
C_r	Reaction rate parameter	$C_r = \frac{K_r^2 (1-et)}{b}$

In Chapter 3, we have already satisfied the mass conservation equation (4.1) identically, and discussed the non-dimensionalization process of the momentum equation (4.2). Here, our focus will be solely on elucidating the non-dimensionalization process of the energy and concentration equations for our fluid problem.

4.3.1 Non-Dimensionalization of Energy Equation

In this section, we discuss the non-dimensionalization process of the energy equation (4.3) for our hybrid nanofluid model. For this equation, the following derivatives are also required.

- $\frac{\partial T^4}{\partial z} = 4T_\infty^3 \frac{\partial T}{\partial z}$.
- $q_r = \frac{-4\sigma^*}{3k^*} \frac{\partial T^4}{\partial z}$.
$$= \frac{-4\sigma^*}{3k^*} \left(4T_\infty^3 \frac{\partial T}{\partial z} \right).$$
$$= \frac{-16\sigma^*}{3k^*} T_\infty^3 \left(\frac{\partial T}{\partial z} \right).$$
$$= \frac{-16\sigma^*}{3k^*} T_\infty^3 \left[(T_w - T_\infty)\theta'(\eta) \sqrt{\frac{b}{(1-et)\nu}} \right].$$

- $\dfrac{\partial q_r}{\partial z} = \dfrac{-16\sigma^*}{3k^*}T_\infty^3\left[(T_w - T_\infty)\sqrt{\dfrac{b}{(1-et)\nu}}\ \right]\dfrac{\partial}{\partial z}\theta'(\eta).$

$= \dfrac{-16\sigma^*}{3k^*}T_\infty^3\left[(T_w - T_\infty)\sqrt{\dfrac{b}{(1-et)\nu}}\ \right]\theta''\sqrt{\dfrac{b}{(1-et)\nu}}.$

$= \dfrac{-16\sigma^*}{3k^*}T_\infty^3(T_w - T_\infty)\dfrac{b}{(1-et)\nu}\theta''(\eta).$

- $v_z = -2v_e R_e^{-\frac{1}{2}} f(\eta).$

$= -2\sqrt{\dfrac{b\nu}{1-et}}f(\eta).$

- $\dfrac{\partial v_z}{\partial t} = \dfrac{\partial}{\partial t}\Big[-2\sqrt{\dfrac{b\nu}{1-et}}f(\eta)\Big].$

$= -2\sqrt{b\nu}\dfrac{\partial}{\partial t}\Big[(1-et)^{-1}f(\eta)\Big].$

$= -2\sqrt{b\nu}\Big[(1-et)^{-1}f'(\eta)\dfrac{\partial \eta}{\partial t} + \Big(e(1-et)^{-2}f(\eta)\Big)\Big].$

$= -2\sqrt{b\nu}\Big[(1-et)^{-1}f'\dfrac{e\eta}{2(1-et)} + \Big(e(1-et)^{-2}f\Big)\Big].$

$= -2\sqrt{b\nu}e\eta f'(\eta) - 2\sqrt{b\nu}e(1-et)^{-2}f(\eta).$

$= \dfrac{-2\sqrt{b\nu}e}{(1-et)^2}\Big[\dfrac{1}{2}f'\eta + f\Big].$

- $\dfrac{\partial v_z}{\partial z} = \dfrac{\partial}{\partial z}\Big(-2\sqrt{\dfrac{b\nu}{1-et}}f(\eta)\Big).$

$= -2\sqrt{\dfrac{b\nu}{1-et}}f'(\eta)\dfrac{\partial \eta}{\partial z}.$

$= -2\sqrt{\dfrac{b\nu}{1-et}}f'(\eta)\sqrt{\dfrac{b}{(1-et)\nu}}.$

$= -2\dfrac{b}{1-et}f'(\eta).$

- $\dfrac{\partial v_z}{\partial r} = \dfrac{\partial}{\partial r}\Big(-2\sqrt{\dfrac{b\nu}{1-et}}f(\eta)\Big).$

$= 0.$

- $\dfrac{\partial^2 T}{\partial r \partial z} = 0.$
- $\dfrac{\partial^2 T}{\partial r \partial t} = 0.$

- $\dfrac{\partial^2 T}{\partial z \partial t} = \dfrac{\partial}{\partial z}\Big(\dfrac{\partial T}{\partial t}\Big).$

$= \dfrac{\partial}{\partial z}\Big(\dfrac{(T_w - T_\infty)\eta e}{2(1-et)}\theta'(\eta)\Big).$

$= \dfrac{T_w - T_\infty}{2(1-et)}e\dfrac{\partial}{\partial z}\Big(\eta\theta'\Big).$

$= \dfrac{T_w - T_\infty}{2(1-et)}e\Big((\eta)\dfrac{\partial}{\partial z}\theta'(\eta) + \theta'(\eta)\dfrac{\partial}{\partial z}(\eta)\Big).$

$= \dfrac{T_w - T_\infty}{2(1-et)}e\Big(\eta\theta''(\eta)\dfrac{\partial}{\partial z}\Big(z\sqrt{\dfrac{b}{(1-et)\nu}}\Big) + \theta'(\eta)\dfrac{\partial}{\partial z}\Big(z\sqrt{\dfrac{b}{(1-et)\nu}}\Big)\Big).$

$$\bullet\ \frac{\partial^2 T}{\partial z \partial t} = \frac{T_w - T_\infty}{2(1-et)} e\left(\eta\theta''(\eta)\frac{\partial}{\partial z}\sqrt{\frac{b}{(1-et)\nu}} + \theta'(\eta)\sqrt{\frac{b}{(1-et)\nu}}\right).$$

$$= \frac{T_w - T_\infty}{2(1-et)} e\sqrt{\frac{b}{(1-et)\nu}}\left(\eta\theta' + \theta'(\eta)\right).$$

$$= \frac{(T_w - T_\infty)e\sqrt{b}}{2\sqrt{(1-et)^3\nu}}\left(\eta\theta''(\eta) + \theta'(\eta)\right).$$

$$= \frac{(T_w - T_\infty)e\sqrt{b}}{2\nu(1-et)^{\frac{3}{2}}}\left(\eta\theta' + \theta'\right).$$

$$\bullet\ \frac{\partial^2 T}{\partial t^2} = \frac{\partial}{\partial t}\left(\frac{\partial T}{\partial t}\right).$$

$$= \frac{\partial}{\partial t}\left(T_w - T_\infty \frac{\eta e}{2(1-et)}\theta'(\eta)\right).$$

$$= \frac{\partial}{\partial t}\left((T_w - T_\infty)\frac{z\sqrt{\frac{b}{(1-et)\nu}}e}{2(1-et)}\theta'(\eta)\right).$$

$$= \frac{\partial}{\partial t}\left((T_w - T_\infty)\frac{z\sqrt{b}e}{2\sqrt{\nu}(1-et)^{\frac{3}{2}}}\theta'(\eta)\right).$$

$$= \frac{\partial}{\partial t}\left((T_w - T_\infty)\frac{z\sqrt{b}e}{2\sqrt{\nu}}(1-et)^{-\frac{3}{2}}\theta'(\eta)\right).$$

$$= (T_w - T_\infty)\frac{z\sqrt{b}e}{2\sqrt{\nu}}\left[(1-et)^{-\frac{3}{2}}\theta''(\eta)\frac{e\eta}{2(1-et)} + \frac{3e}{2}(1-et)^{-\frac{5}{2}}\theta'(\eta)\right].$$

$$= (T_w - T_\infty)\frac{z\sqrt{b}e^2}{4\sqrt{\nu}(1-et)^{\frac{5}{2}}}\left[\theta''\eta + 3\theta'(\eta)\right].$$

Now, we substitute the above partial derivatives into the equation (4.3)

$$(T_w - T_\infty)\frac{e\eta}{2(1-et)}\theta' + \left(-2\sqrt{\frac{b\nu}{1-et}}f\right)\left[(T_w - T_\infty)\theta'(\eta)\sqrt{\frac{b}{(1-et)\nu}}\theta'\right]$$

$$+ \beta_T\left[\frac{\eta e^2}{4(1-et)^2}(T_w - T_\infty)(\eta\theta'' + 3\theta'(\eta)) - 2f\sqrt{\frac{b\nu}{1-et}}\frac{(T_w - T_\infty)\sqrt{b}e}{\sqrt{\nu}(1-et)^{\frac{3}{2}}}\left(\eta\theta''(\eta) + \theta'(\eta)\right)\right.$$

$$\left. - e\sqrt{\frac{b\nu}{1-et}}\left[\frac{f'\eta}{1-et} + \frac{f(\eta)}{(1-et)}\right]\left((T_w - T_\infty)\sqrt{\frac{b}{(1-et)\nu}}\theta'(\eta)\right)\right.$$

$$\left. + 4\frac{b^2\nu}{(1-et)^2}f(\eta)f'(\eta)\left((T_w - T_\infty)\sqrt{\frac{b}{(1-et)\nu}}\theta'\right)\right.$$

$$= \frac{k_{hnf}}{(\rho c_p)_{hnf}}\left[\frac{b}{(1-et)\nu}\ (T_w - T_\infty)\theta''(\eta)\right] + \frac{1}{(\rho c_p)_{hnf}}\left[\frac{16\sigma^* T_\infty^3}{3k^*}(T_w - T_\infty)\frac{b}{(1-et)\nu}\theta''\right].$$

$$\Rightarrow \frac{e\eta}{2(1-et)}\theta' - 2\frac{b}{1-et}f\theta' + \beta_T\left[\frac{\eta e^2}{4(1-et)^2}(\eta\theta'' + 3\theta') - \frac{2be}{(1-et)^2}f(\eta\theta'' + \theta')\right.$$

$$\left. - \frac{cbf'}{(1-et)^2}\theta'' - \frac{be}{(1-et)^2}f\theta' + \frac{4b^2}{(1-et)^2}ff'\theta' + \frac{4b^2}{(1-et)^2}f^2\theta''\right]$$

$$= \frac{k_{hnf}}{(\rho c_p)_{hnf}}\left[\frac{b}{(1-et)\nu}\ \theta''(\eta)\right] + \frac{1}{(\rho c_p)_{hnf}}\left[\frac{16\sigma^* T_\infty^3}{3k^*}\frac{b}{(1-et)\nu}\theta''\right].$$

$$\Rightarrow \frac{\eta e}{2b}\theta' - 2f\theta' + \beta_T\frac{b}{1-et}\left[\frac{\eta e^2}{4b^2}(\eta\theta'' + 3\theta') - 2\frac{e}{b}f(\eta\theta'' + \theta') - \frac{e}{b}\eta f'\theta' - \frac{e}{b}f\theta' + 4ff'\theta' + 4f^2\theta''\right].$$

$$= \frac{k_{hnf}}{(\rho c_p)_{hnf}}\left[\frac{b}{(1-et)\nu}\ \theta''(\eta)\right]\frac{1}{(\rho c_p)_{hnf}}\left[\frac{16\sigma^* T_\infty^3}{3k^*}\frac{b}{(1-et)\nu}\theta''\right].$$

$$\Rightarrow \frac{\eta e}{2b}\theta' - 2f\theta' + \beta_T \frac{b}{1-et}\left[\frac{\eta e^2}{4b^2}(\eta\theta'' + 3\theta') - 2\frac{e}{b}f(\eta\theta''(\eta) + \theta'(\eta)) - \frac{e}{b}\eta f'\theta'(\eta) - \frac{e}{b}f\theta'(\eta)\right.$$
$$\left. + 4ff'\theta'(\eta) + 4f^2\theta''(\eta)\right] = \frac{\frac{k_{hnf}}{k_f}}{Pr\frac{(\rho c_p)_{hnf}}{(\rho c_p)_f}}\left[\left(1 + \frac{4}{3}Rd\right)\right]\theta''(\eta).$$
$$\Rightarrow \frac{k_{hnf}/k_f}{(\rho c_p)_{hnf}/(\rho c_p)_f}\left[\left(1 + \frac{4}{3}Rd\right)\right]\theta'' + Pr\left(2f - \frac{\eta}{2}\beta\right)\theta'(\eta) - Pr\delta_T\left[\frac{\eta}{4}\beta^2\eta\theta'' + \frac{\eta}{4}\beta^2 3\theta'(\eta)\right.$$
$$\left. - 2\beta f\eta\theta''(\eta) - 2\beta f\theta' - \beta\eta f'\theta' - \beta f\theta' + 4ff'\theta' + 4f^2\theta''\right] = 0.$$
$$\Rightarrow \frac{k_{hnf}/k_f}{(\rho c_p)_{hnf}/(\rho c_p)_f}\left[\left(1 + \frac{4}{3}Rd\right)\right]\theta''(\eta) + Pr\left(2f - \frac{\eta}{2}\beta\right)\theta'(\eta) - Pr\delta_T\left[\frac{1}{4}(\beta^2\eta^2\theta'' + 3\eta\theta'(\eta)\right.$$
$$\left. - \beta\left(2f\theta''(\eta) + 3f\theta'(\eta) + f\theta'(\eta)\right) + 4ff'\theta'(\eta) + 4f^2\theta''(\eta)\right] = 0. \tag{4.7}$$

4.3.2 Non-Dimensionalization of Concentration Equation

Here, we focus on the non-dimensionalization process specifically applied to the concentration equation (4.4) in our hybrid nanofluid model. For this purpose, the following derivatives are also required.

$$\phi(\eta) = \frac{C - C_\infty}{C_\infty}.$$
$$C = C_\infty\left(\phi(\eta) + C_\infty\right).$$
- $$\frac{\partial C}{\partial t} = C_\infty\phi'(\eta)\frac{\partial \eta}{\partial t}.$$
$$= C_\infty\phi'(\eta)\frac{C\eta}{2(1-et)}.$$
$$= \frac{C_\infty e\eta}{2(1-et)}\phi'(\eta).$$
$$\frac{\partial C}{\partial r} = C_\infty\phi'(\eta)\frac{\partial \eta}{\partial r}.$$
$$= 0.$$

(4.8)

- $$\frac{\partial C}{\partial z} = C_\infty\phi'(\eta)\frac{\partial \eta}{\partial z}.$$
$$\frac{\partial C}{\partial z} = C_\infty\phi'(\eta)\sqrt{\frac{b}{(1-et)\nu}}.$$
- $$\frac{\partial^2 C}{\partial z^2} = C_\infty\phi''(\eta)\sqrt{\frac{b}{(1-et)\nu}}\frac{\partial \eta}{\partial z}.$$
$$\frac{\partial^2 C}{\partial z^2} = C_\infty\phi''(\eta)\sqrt{\frac{b}{(1-et)\nu}}\sqrt{\frac{b}{(1-et)\nu}}.$$

(4.9)

$$T = (T_w - T_\infty)\theta(\eta) + T_\infty.$$
$$\frac{T}{T_\infty} = \left(\frac{T_w}{T_\infty} - 1\right)\theta + 1.$$
$$T = T_\infty\left(1 + (\theta_w - 1)\theta\right).$$

Upon substituting the corresponding derivatives into the concentration equation (4.4), it takes the following form:

$$\begin{aligned}
&\frac{C_\infty e\eta}{2(1-et)}\phi'(\eta) - 2\left(\sqrt{\frac{b\nu}{1-et}}f(\eta)\right)\left(C_\infty\sqrt{\frac{b}{(1-et)\nu}}\phi'\right)\\
&= D_B\frac{bC_\infty}{(1-et)\nu}\phi'' + \frac{D_T}{T_\infty}(T_w-T_\infty)\frac{b}{(1-et)\nu}\theta''\\
&- K_r^2(C_\infty\phi + C_\infty - C_\infty)\Big(1+(\theta_w-1)\theta\Big)^m\exp\left(\frac{-E_a}{K_1(T_\infty(1+(\theta_w-1)\theta))}\right).\\
\Rightarrow\ &\frac{C_\infty e\eta}{2(1-et)}\phi'(\eta) - \frac{2bC_\infty}{1-et}f(\eta)\phi'(\eta) = D_B\frac{bC_\infty}{(1-et)\nu}\phi'' + \frac{D_T}{T_\infty}(T_w-T_\infty)\frac{b}{(1-et)\nu}\theta''\\
&- K_r^2(C_\infty\phi)\Big(1+(\theta_w-1)\theta\Big)^m\exp\left(\frac{-E_a}{K_1T_\infty(1+(\theta_w-1)\theta)}\right).\\
\Rightarrow\ &\frac{1}{2}\eta\beta\phi' - 2f\phi' = \frac{1}{Sc}\phi'' + \frac{D_T(T_w-T_\infty)}{T_\infty C_\infty\nu}\frac{\tau D_B\nu}{\tau D_B\nu}\theta''\\
&- C_r\phi\Big(1+(\theta_w-1)\theta\Big)^m\exp\left(\frac{-E_a}{K_1T_\infty(1+(\theta_w-1)\theta)}\right).\\
\Rightarrow\ &\frac{1}{2}\eta\beta\phi' - 2f\phi' = \frac{1}{Sc}\phi'' + \frac{\tau D_T(T_w-T_\infty)}{T_\infty C_\infty\nu}\frac{\nu}{\tau D_B C_\infty}\frac{D_B}{\nu}\theta''\\
&- C_r\phi\Big(1+(\theta_w-1)\theta\Big)^m\exp\left(\frac{-E}{1+(\theta_w-1)\theta}\right).\\
\Rightarrow\ &\frac{1}{2}\eta\beta\phi' - 2f\phi' = \frac{1}{Sc}\phi'' + \frac{Nt}{Nb}\frac{1}{Sc}\theta'' - C_r\phi\Big(1+(\theta_w-1)\theta\Big)^m\exp\left(\frac{-E}{1+(\theta_w-1)\theta}\right).\\
\Rightarrow\ &\frac{1}{2}\eta\beta\phi' - 2f\phi' = \frac{1}{Sc}\phi'' + \frac{Nt}{Nb}\frac{1}{Sc}\theta''(\eta) - C_r\phi\Big(1+(\theta_w-1)\theta\Big)^m\exp\left(\frac{-E}{1+(\theta_w-1)\theta}\right).\\
\Rightarrow\ &\phi'' + \frac{Nt}{Nb}\theta'' - ScC_r\phi\Big(1+(\theta_w-1)\theta\Big)^m\exp\left(\frac{-E}{1+(\theta_w-1)\theta}\right) = 0. \qquad (4.10)
\end{aligned}$$

4.3.3 Dimensionless form of Boundary Conditions

The corresponding boundary conditions of the momentum equation (4.2) and energy equation (4.3) have already been non-dimensionalized in the previous Chapter 3. The boundary condition of the concentration equation (4.4) are transformed into its non-dimensional form through the following procedure:

$$\begin{aligned}
\bullet\quad & D_B\frac{\partial C}{\partial y} + \frac{D_T}{T_\infty}\frac{\partial T}{\partial y} = 0 && at\quad y=0.\\
\Rightarrow\ & D_B\frac{a}{\nu_f}\left(C_f - C_\infty\right)\phi'(\eta) + \frac{D_T}{T_\infty}\left(T_w - T_\infty\right)\frac{a}{\nu_f}\phi'(\eta) = 0, && at\quad \eta=0.\\
\Rightarrow\ & D_B\left(C_f - C_\infty\right)\phi'(\eta) + \frac{D_T}{T_\infty}\left(T_w - T_\infty\right)\phi'(\eta) = 0, && at\quad \eta=0.\\
\Rightarrow\ & Nb\phi'(\eta) + Nt\theta'(\eta) = 0, && at\quad \eta=0.\\
\bullet\quad & C \longrightarrow C_\infty, && as\quad y\longrightarrow\infty.\\
\Rightarrow\ & \left(C_f - C_\infty\right)\phi'(\eta) + C_\infty \longrightarrow C_\infty, && as\quad \eta\longrightarrow\infty.\\
\Rightarrow\ & \left(C_f - C_\infty\right)\phi'(\eta) \longrightarrow C_\infty, && as\quad \eta\longrightarrow\infty.
\end{aligned}$$

$$\Rightarrow \quad \phi'(\eta) \longrightarrow 0, \qquad as \quad \eta \longrightarrow \infty.$$

4.4 Solution Framework

The numerical solution of the momentum equation (4.2) has already been obtained and discussed in Chapter 3. To find numerical solutions for equation (4.3.1) using the shooting method, we assume f, f', and f'' as the known functions. The following notations have been used for the implementation of the shooting method:

In order to solve the ODE (4.3.1), the following notations are considered as an initial step:

$$\theta(\eta) = Y_1, \qquad \theta'(\eta) = Y_1' = Y_2.$$

The following system of first order ODEs has been obtained to replace the momentum equation:

$$\begin{aligned} Y_1' &= Y_2, & Y_1(0) &= 0, \\ Y_2' &= \frac{Pr\delta_T\left[\frac{3}{4}\eta Y_1 - \beta\left(3fY_2 + fY_2\right) + 4ff'Y_2\right] - Pr\left(2f - \frac{\eta}{2}\beta\right)Y_2}{\frac{K_{hnf/K_f}}{(\rho c_p)_{hnf}/(\rho c_p)_f}\left(1 + \frac{4}{3}Rd\right) - \frac{Pr}{4}\delta_T\beta^2\eta^2 + 2f\beta Pr\delta_T - 4Pr\delta_T f^2}. & Y_2(0) &= P_1. \end{aligned}$$

To utilize the Runge-Kutta 4th order (RK4) method for the numerical solution of the mentioned initial value problem, the domain of our problem is considered to be bounded, i.e., $[0, \eta]$ where $\eta = \eta_\infty$ the condition P_1 within the system of equations need to be carefully chosen. The choice of missing condition P_1 is such that

$$Y_2\left(\eta_\infty, P_1\right) = 0.$$

Newton's method will be used to further refine the selection of P_1. This method has the following iterative scheme:

$$P_1{}^{(m+1)} = P_1^{(m)} - \frac{Y_2\left(\eta_\infty, P_1^{(m)}\right)}{\left(\frac{\partial}{\partial P_1}Y_2\left(\eta_\infty, P_1\right)\right)^{(m)}}.$$

We further introduce the following notations:

$$\frac{\partial Y_1}{\partial P_1} = Y_3, \qquad \frac{\partial Y_2}{\partial P_1} = Y_4.$$

The result from the above new notations, the Newton's iterative scheme is:

$$P_1{}^{(m+1)} = P_1^{(m)} - \frac{Y_2\left(\eta_\infty, P_1^{(m)}\right)}{Y_5\left(\eta_\infty, P_1\right)}.$$

Now differentiating the above system of three first order ODEs with respect to P_1, we get another system of ODEs, as follows:

$$\begin{aligned} Y_3' &= Y_5, && Y_3(0) = 0, \\ Y_4' &= \frac{Pr\delta_T\left[\frac{3}{4}\eta Y_3 - \beta\left(3fY_4 + fY_2\right) + 4ff'Y_4\right] - Pr\left(2f - \frac{\eta}{2}\beta\right)Y_4}{\frac{K_{hnf/K_f}}{(\rho c_p)_{hnf}/(\rho c_p)_f}\left(1 + \frac{4}{3}Rd\right) - \frac{Pr}{4}\delta_T\beta^2\eta^2 + 2f\beta Pr\delta_T - 4Pr\delta_T f^2}. && Y_4(0) = 1. \end{aligned}$$

The stopping rules for Newton's method are outlined as:

$$|Y_2\left(\eta_\infty, P_1\right)| < \epsilon.$$

Now, to solve equation (4.10) numerically by using shooting method, assume f, f', f'', θ and θ' as known functions.

In order to solve the ODE (4.10), the following notations have been considered, as an initial step:

$$\phi(\eta) = Z_1, \qquad \phi'(\eta) = Z_1' = Z_2.$$

The following system of first order ODEs has been obtained to replace the momentum equation:

$$\begin{aligned} Z_1' &= Z_2, && Z_1(0) = q_1, \\ Z_2' &= ScCr\left(1 + \left(\theta_w - 1\right)\theta\right)^m exp\left(\frac{-E}{1 + \left(\theta_w - 1\right)\theta}\right) Z_1 \\ &\quad - \frac{Nt}{Nb}\frac{Pr\delta_T\left[\frac{3}{4}\eta\theta - \beta\left(3f\theta' + f\theta'\right) + 4ff'Y_2\right] - Pr\left(2f - \frac{\eta}{2}\beta\right)\theta'}{\frac{K_{hnf/K_f}}{(\rho c_p)_{hnf}/(\rho c_p)_f}\left(1 + \frac{4}{3}Rd\right) - \frac{Pr}{4}\delta_T\beta^2\eta^2 + 2f\beta Pr\delta_T - 4Pr\delta_T f^2}. && Z_2(0) = -\frac{Nt}{Nb}\theta'(0). \end{aligned}$$

To utilize the Runge-Kutta 4th order (RK4) method for the numerical solution of the mentioned initial value problem, the condition s_1 within the system of equations need to be carefully chosen. The missing condition s_1 needs to be selected so that

$$Z_2\big(\eta_\infty, q_1\big) = 0.$$

Newton's method will be used to further refine the selection of s_1. This method has the following iterative scheme:

$${q_1}^{(m+1)} = q_1^{(m)} - \frac{Z_2\big(\eta_\infty, q_1^{(m)}\big)}{\left(\frac{\partial}{\partial q_1}Z_2\big(\eta_\infty, q_1\big)\right)^{(m)}}.$$

We further introduce the following notations:

$$\frac{\partial Z_1}{\partial q_1} = Z_3, \qquad \frac{\partial Z_2}{\partial q_1} = Z_4.$$

As a result these of new notations, the Newton's iterative scheme gets the form:

$$q_1{}^{(m+1)} = q_1^{(m)} - \frac{Z_2\big(\eta_\infty, q_1^{(m)}\big)}{Z_5\big(\eta_\infty, q_1\big)}.$$

Now differentiating the above system of three first order ODEs with respect to s_1, we get another system of ODEs, as follows:

$$Z_3' = Z_4, \qquad Z_3(0) = 1,$$
$$Z_4' = ScCr\,(1 + (\theta_w - 1)\,\theta)^m\, exp\left(\frac{-E}{1 + (\theta_w - 1)\,\theta}\right) Z_3. \qquad Z_4(0) = 0.$$

The criteria for terminating Newton's technique is defined as:

$$|Z_2\,(\eta_\infty, q_1)| < \epsilon,$$

4.5 Results Interpretation

After transforming the governing PDEs describing the fluid flow into a system of ODEs, several crucial parameters emerge. The impact of these physical parameters on the velocity $f'(\eta)$, temperature $\theta(\eta)$, and concentration of nanoparticle $\phi(\eta)$ is thoroughly investigated through the use of graphical representations. The significance and interpretations the impact of each parameter in this study are discussed in detail, and the study's results are comprehensively presented.

4.5.1 Analysis of Computational Results

This section presents the computational findings concerning the Nusselt number and Skin friction across various dimensionless parameters. An increase in the magnetic number M, indicating the strength of the magnetic field, is observed to induce a reduction in the Nusselt number, suggesting a suppression of the convective heat transfer. Similarly, heightened values of the unsteadiness parameter β signify the increased flow fluctuations, contributing to a diminished Nusselt number due to disrupted heat transfer processes. Additionally, elevated levels of the thermal radiation parameter Rd are associated with lower Nusselt numbers, highlighting the impact of radiative heat transfer mechanisms on the overall convective heat transfer rate.

Conversely, an augmentation in the suction parameter S amplifies fluid extraction from the boundary layer, consequently enhancing the heat transfer rates and leading to an increased Nusselt number. Likewise, an increase in the thermal time relaxation parameter δ_T indicates a faster response of the fluid temperature to changes in the boundary conditions, resulting in heightened convective heat transfer and thus, an elevated Nusselt number. Furthermore,an augmentation in the stretching parameter λ correlates with the intensified fluid motion and stretching, fostering enhanced heat transfer and a subsequent increase in the Nusselt number.

TABLE 4.3: The numerical result of embedded parameters on local Nusselt and $\phi(0)$, respectively. $Pr = 6.2$ when $\phi_{Al} = 0.02$ and $\phi_{Cu} = 0.02$

.

M	β	S	λ	Rd	δ_T	Nt	Nb	Sc	C_r	E	m	θ_w	$Re_x^{-1/2}Nu_x$	$\phi(0)$
0.2	0.2	0.1	0.2	1.2	0.001	0.1	0.2	3	0.5	0.0	1	1.1	1.577074	-0.3951294
0.4													1.584193	-0.3955440
0.6													1.590881	-0.3959229
0.8													1.597187	-0.3962799
	0.3												1.550533	-0.3956009
	0.6												1.468260	-0.3973533
	0.8												1.410217	-0.3987446
		0.2											1.915940	-0.4112352
		0.4											2.657683	-0.4222855
		0.6											3.4637507	-0.4222987
			0.4										1.723998	-0.4031434
			0.6										1.860964	-0.4088434
			0.8										1.989579	-0.4130009
				0.5									2.003257	-0.4984499
				0.7									1.846839	-0.4607399
				0.9									1.722763	-0.4306562
					0.002								1.577815	-0.3954238
					0.003								1.577855	-0.3957402
					0.004								1.579296	-0.3960860
						0.2							1.577074	-0.7902588
						0.3							1.577074	-1.1853883
						0.4							1.577074	-1.5805177
							0.3						1.577074	-0.2634196
							0.4						1.577074	-0.1975647
							0.5						1.577074	-0.1580517
								5					1.577074	-0.2913039
								7					1.577074	-0.2362829
								9					1.577074	-0.2010648
									1				1.577074	-0.3309495
									1.5				1.577074	-0.2886524
									2				1.577074	-0.2584227
										0.5			1.577074	-0.4287835
										1			1.577074	-0.4539922
										2			1.577074	-0.4839134
											2		1.577074	-0.3895190
											4		1.577074	-0.3776002
											8		1.577074	-0.3510107
												1.3	1.577074	-0.3848644
												1.5	1.577074	-0.3752079
												1.9	1.577074	-0.3575137

4.5.2 Velocity Profile

Figures 4.1 to 4.4 provide insights into the nature of the velocity profile, denoted as $f'(\eta)$, with respect to various physical parameters. Specifically, Figure 4.1 and 4.2 illustrate the effects of the magnetic force M and unsteadiness parameter (β) on the dimensionless velocity $f'(\eta)$. It is evident that both of the nanofluids, namely Al_2O_3/H_2O and Al_2O_3-Cu/H_2O, experience a significant decrease in flow velocity as the values of these two parameters M and β increase.

Variation in the magnetic field parameter M results in a noticeable decline in the flow velocity across the fluid domain, indicating the influence of the applied magnetic field. This phenomenon is associated with the generation of the Lorentz force, resembling a drag force, within electrically conductive fluids. Similarly, increasing the unsteady parameter β results in a decrease in the velocity profiles, along with a reduction in the momentum boundary layer thickness in both scenarios. This indicates that the unsteadiness parameter diminishes the flow rate associated with the stretching sheet.

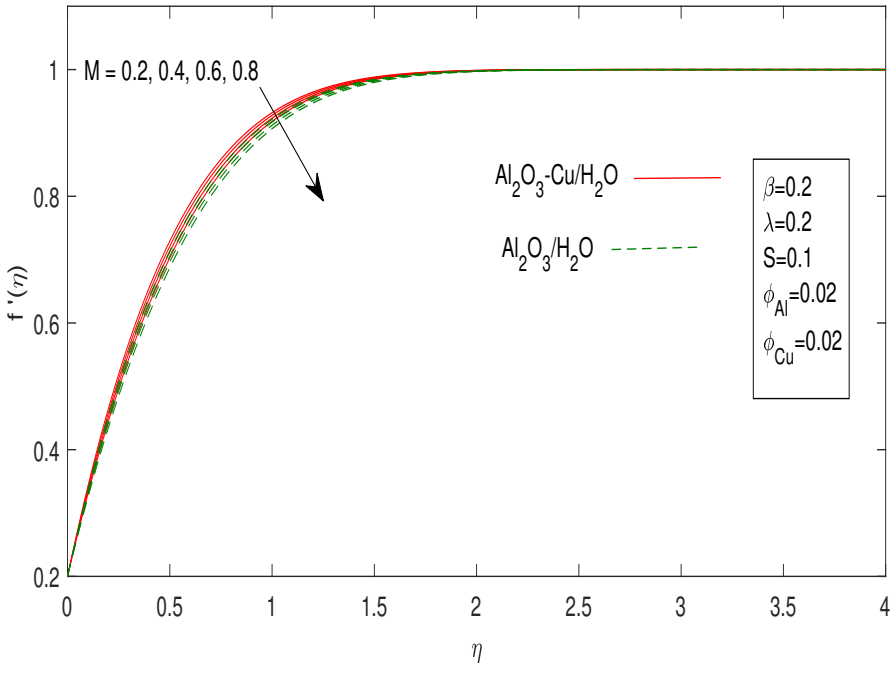

FIGURE 4.1: Influence of M on velocity profile $f'(\eta)$

Figures 4.3 and 4.4 illustrate significant findings regarding the impact of the suction/injection parameter (S) and stretching parameter (λ) on the velocity profile $f'(\eta)$. The analysis reveals that variations in both S and λ result in a reduction in fluid velocity.

It's noticeable that as the suction parameter $S > 0$ rises, there is a significant decrease in velocity, whereas fluid velocity increases with injection $S < 0$. Likewise, the velocity increases with the increasing stretching parameter λ. In conclusion, a higher stretching parameter increases the compression rate of the fluid, resulting a decline in fluid velocity.

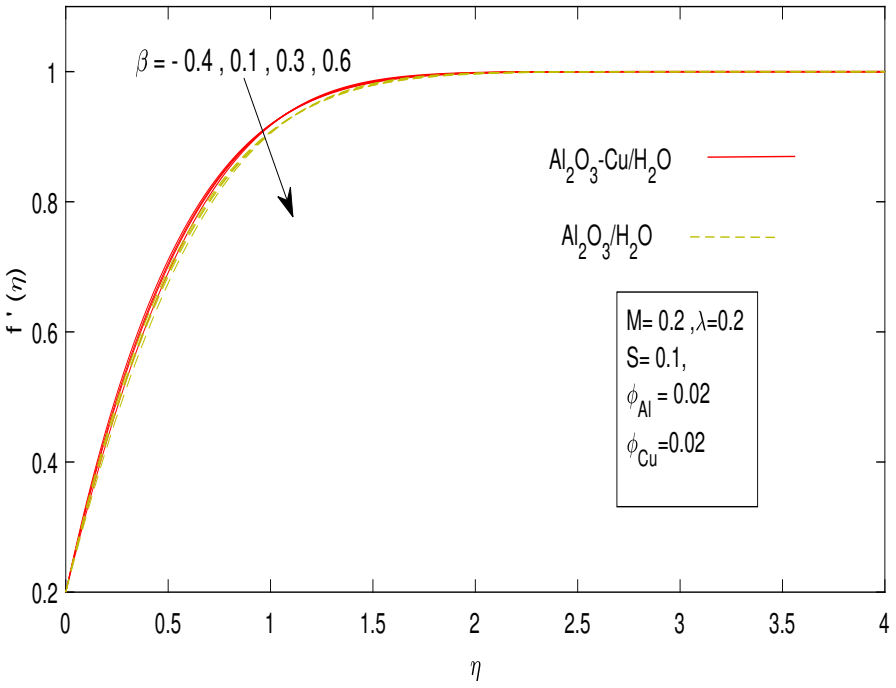

FIGURE 4.2: Influence of β on velocity profile $f'(\eta)$

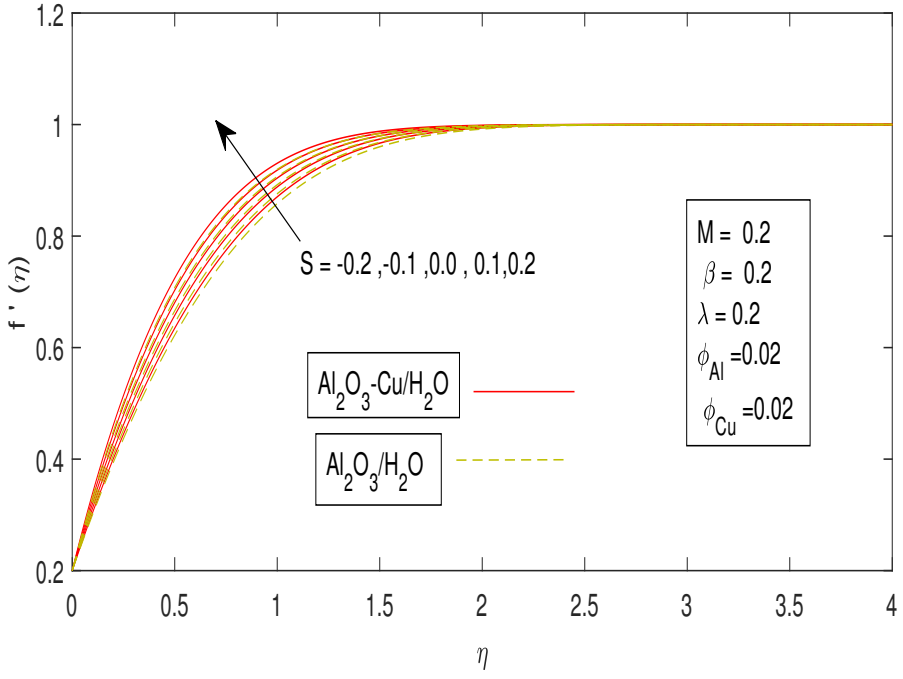

FIGURE 4.3: Influence of S on velocity profile $f'(\eta)$

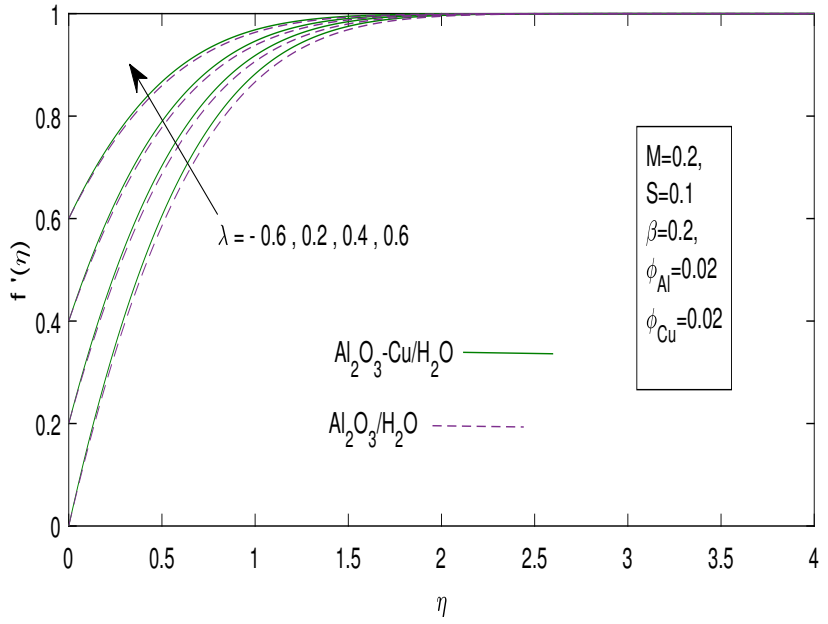

FIGURE 4.4: Influence of λ on velocity profile $f'(\eta)$

4.5.3 Temperature Profile

In this study, we analyze the impact of various physical parameters on the temperature distribution, denoted as $\theta(\eta)$, for two different fluids. As expected, the magnetic field parameter (M) led to a rise in temperature profile (Figure. 4.5) due to the Lorentz force impeding fluid motion and generating internal friction.

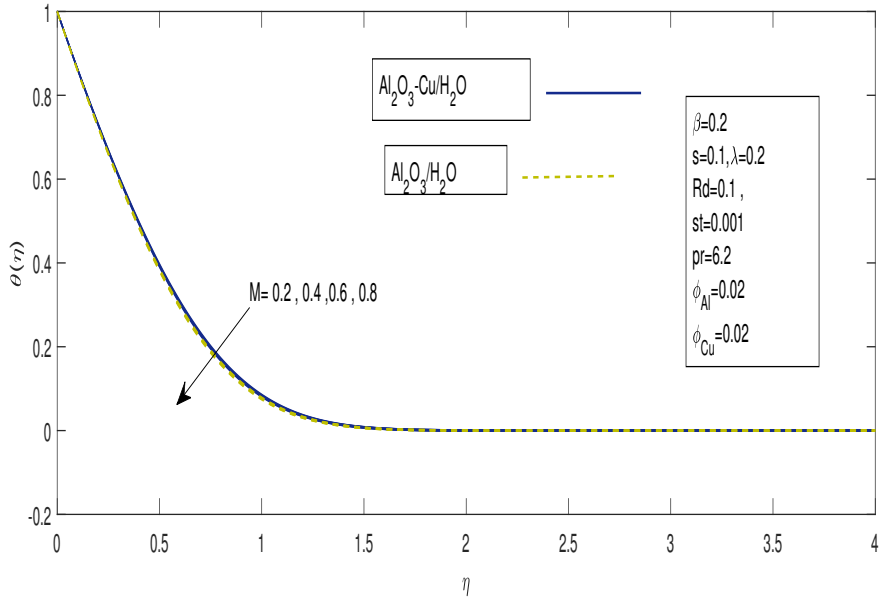

FIGURE 4.5: Influence of M on profile $\theta(\eta)$

Similarly, a higher stretching parameter λ in Figure 4.6 intensified the interaction between the stretching sheet and the fluid, causing a temperature increase. Thermal radiation (Rd) also played a role in elevating temperature (Figure. 4.7) by acting as an additional heat source within the fluid.

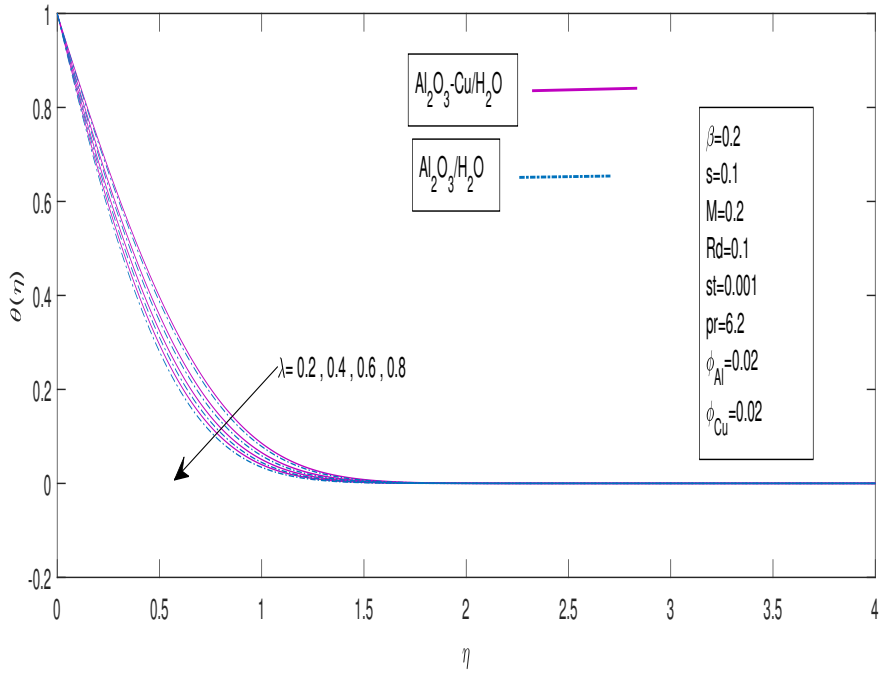

FIGURE 4.6: Influence of λ on profile $\theta(\eta)$

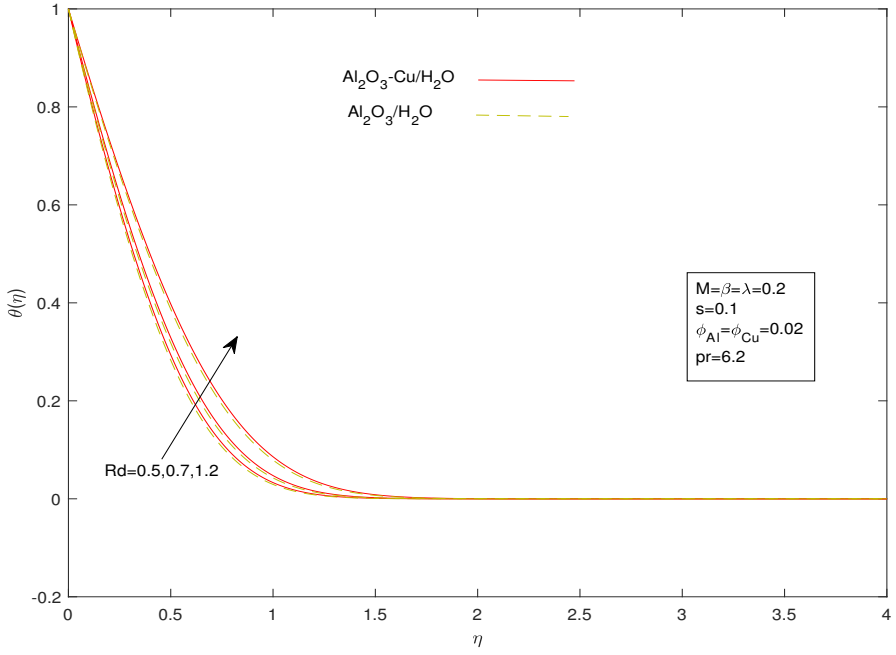

FIGURE 4.7: Influence of Rd on profile $\theta(\eta)$

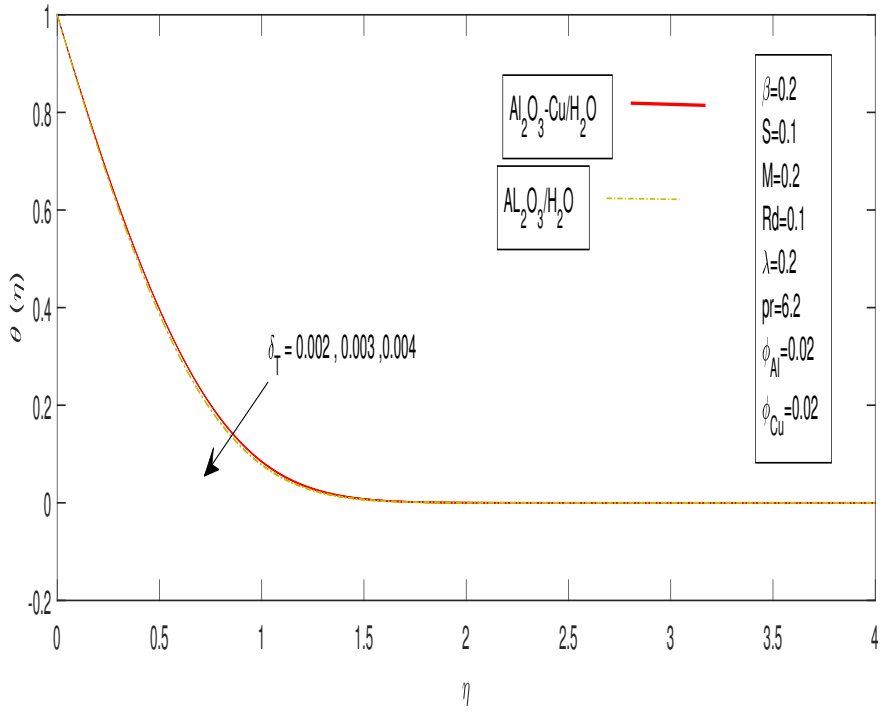

FIGURE 4.8: Influence of δ_T on profile $\theta(\eta)$

4.5.4 Analysis of the Concentration Profile

An analysis of the concentration profiles revealed some interesting interactions between the solutes (dissolved nanoparticles) and various parameters. The magnetic field parameter (M), while increasing the temperature profile, also led to a rise in the concentration profile (Figure 4.9). This might be attributed to the Lorentz force, which not only impedes fluid motion but also influences the movement of nanoparticles. The Lorentz force can trap the nanoparticles within the boundary layer, leading to a higher concentration closer to the stretching sheet.

The stretching parameter λ depicted in Fig. Figure 4.10 exhibits a similar trend, with a higher value leading to an increased concentration profile. This can be explained by the stronger interaction between the stretching sheet and the fluid at higher stretching velocities. This interaction not only affects the fluid flow but also the nanoparticle distribution, leading to a more concentrated layer near the sheet.

Thermal radiation (Rd) maintained its role in enhancing concentration, as shown in Figure 4.11. As the thermal radiation parameter increases, the additional heat source

not only elevates the temperature but can also influence the thermophoretic force. Thermophoresis is a phenomenon where nanoparticles migrate from hot to cold regions. In this case, the increased thermal radiation might create a stronger thermophoretic force driving the nanoparticles towards the cooler region near the stretching sheet, consequently increasing the concentration profile there.

The rising trends observed for unsteadiness parameter (β) in Figure 4.12 and activation energy parameter (E) in Figure 4.13 suggest that these parameters promote a higher concentration profile. While the exact mechanisms might require further investigation. It is possible that these parameters influence the Brownian motion of the nanoparticles or their interaction with the base fluid, leading to a more concentrated layer near the sheet. Finally, the Brownian motion parameter (Nb) in Figure 4.14 contributes to a higher concentration profile for both nanofluid and hybrid nanofluid. This aligns with the concept of Brownian motion, where the random movement of nanoparticles naturally leads to a higher concentration near the surface compared to the bulk fluid.

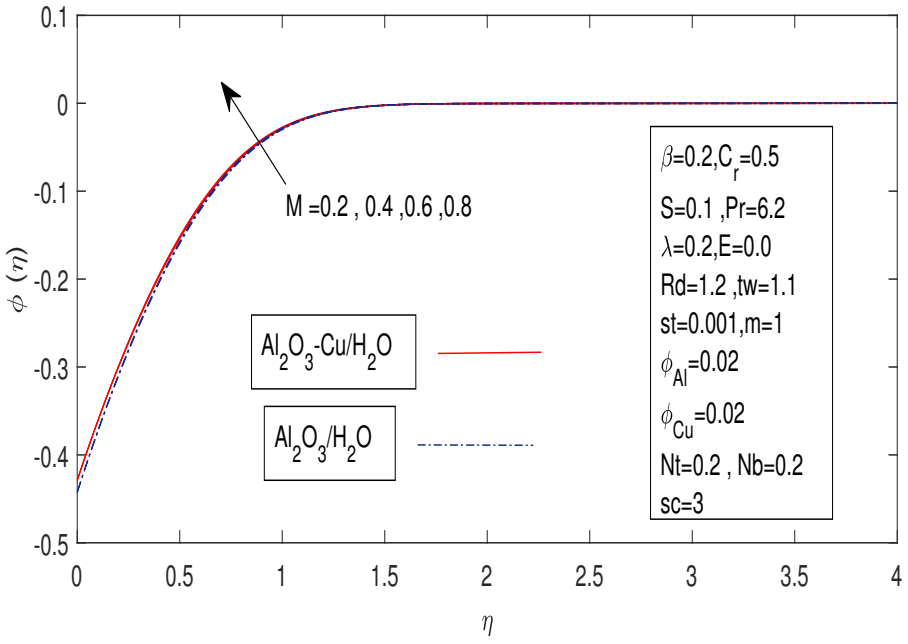

FIGURE 4.9: Influence of M on profile $\phi(\eta)$

Furthermore, Figure 4.15 showcases the influence of the Schmidt number (Sc) on the concentration profile. The Schmidt number represents the ratio of momentum diffusivity to mass diffusivity. A lower Sc value signifies a higher mass diffusivity, meaning the nanoparticles can diffuse more readily within the fluid. This explains the observed enhancement in concentration profile for both fluids with a lower Sc. Conversely, a

higher Sc value (lower mass diffusivity) hinders the nanoparticle movement, leading to a less concentrated profile near the stretching sheet.

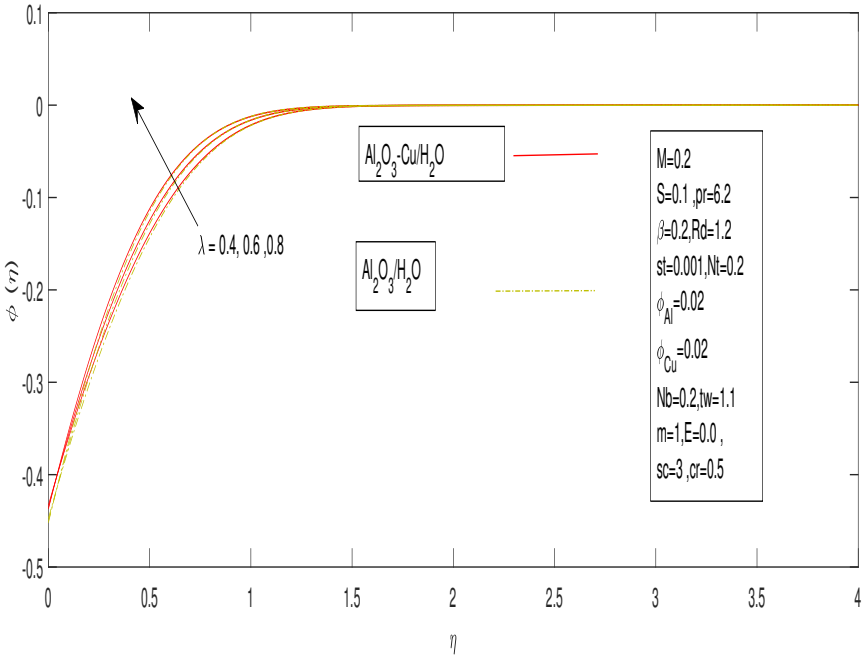

FIGURE 4.10: Influence of λ on profile $\phi(\eta)$

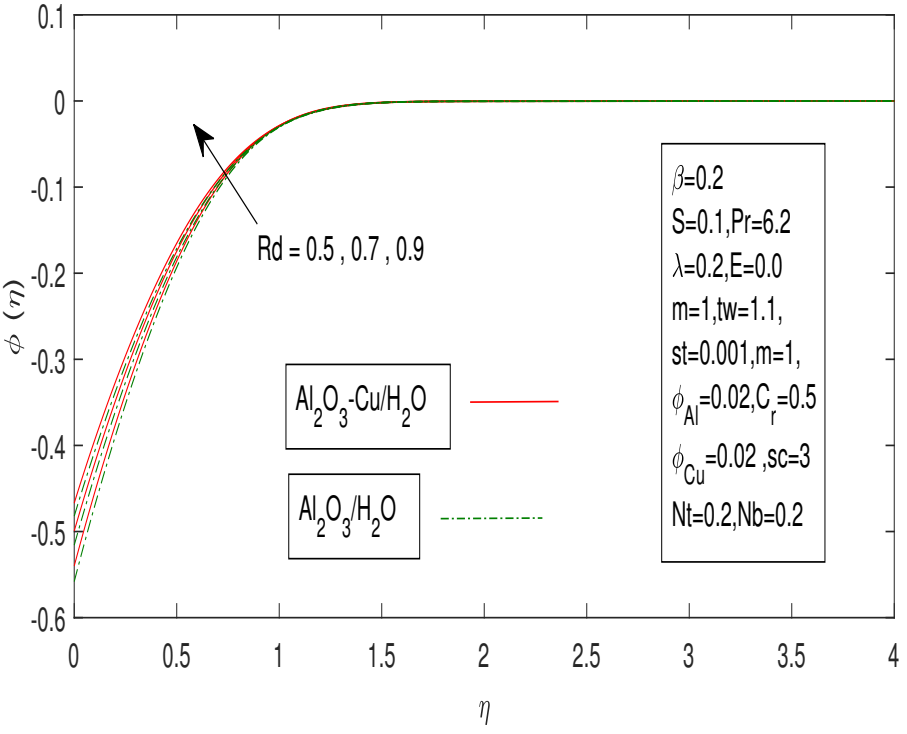

FIGURE 4.11: Influence of Rd on profile $\phi(\eta)$

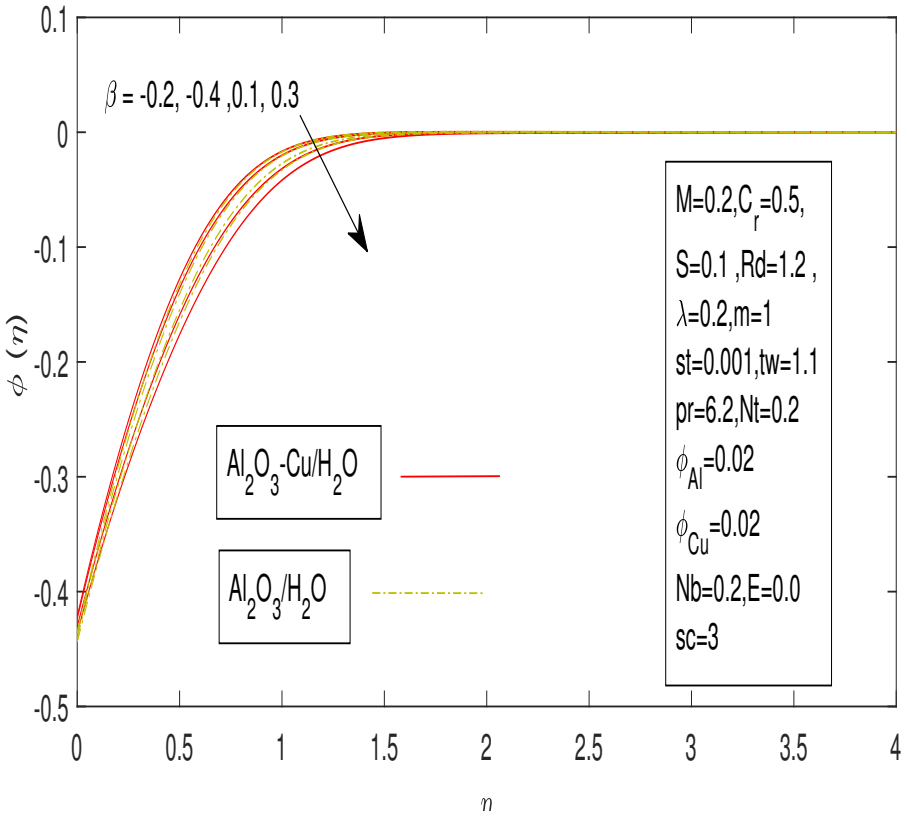

FIGURE 4.12: Influence of β on profile $\phi(\eta)$

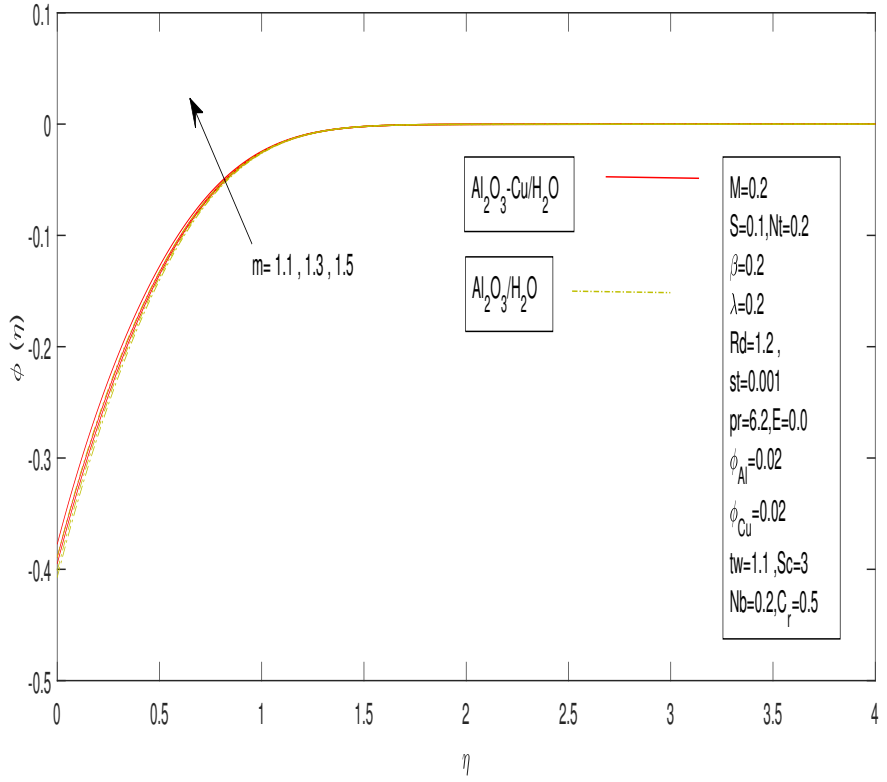

FIGURE 4.13: Influence of m on profile $\phi(\eta)$

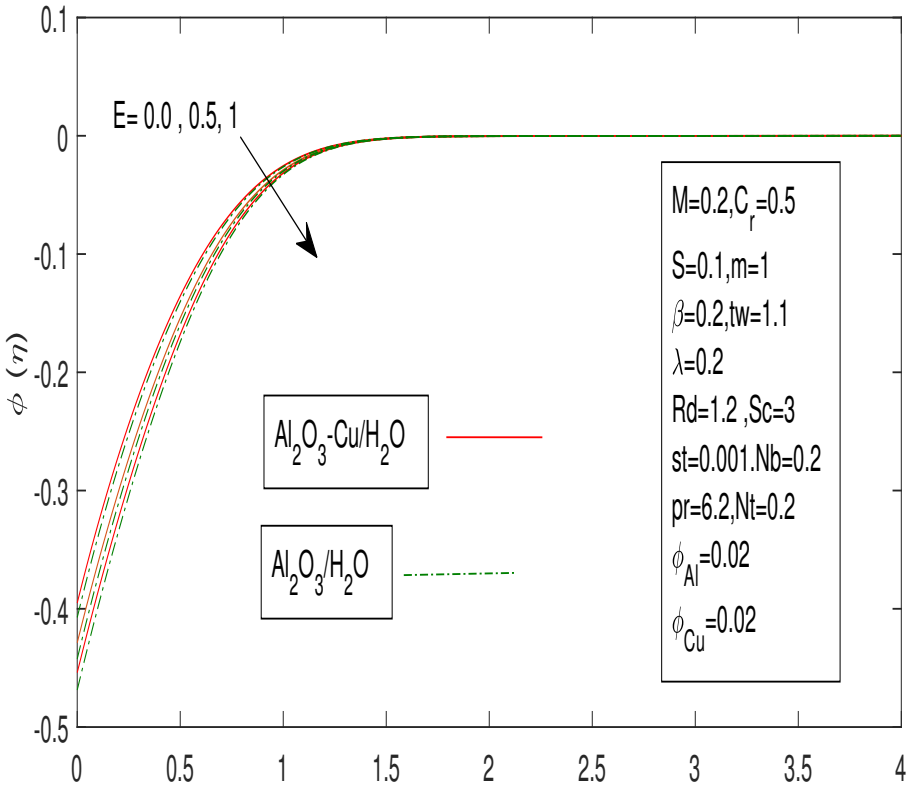

FIGURE 4.14: Influence of E on profile $\theta(\eta)$

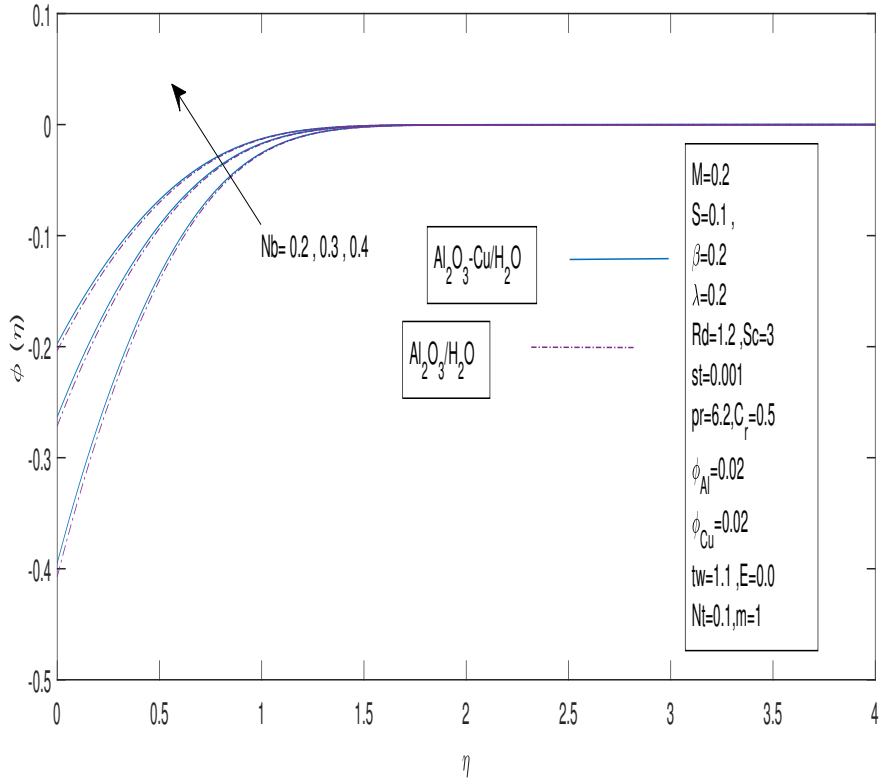

FIGURE 4.15: Influence of Nb on profile $\phi(\eta)$

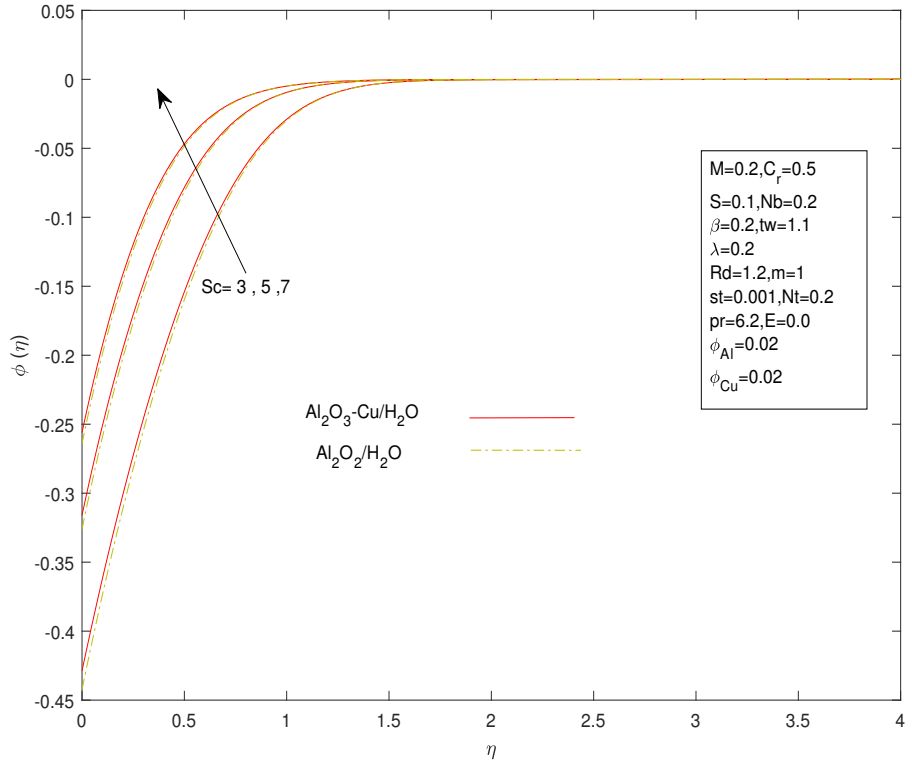

FIGURE 4.16: Influence of Sc on profile $\theta(\eta)$

Finally, Figure 4.17 depicts the effect of the thermal time relaxation parameter (δ_T) on the concentration profile. Interestingly, it exhibits an opposite trend compared to its

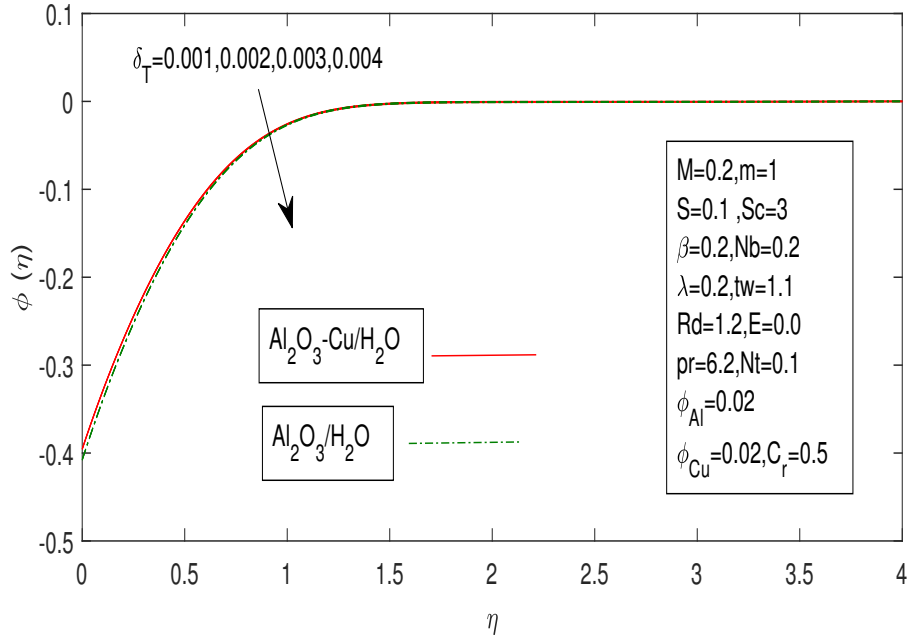

FIGURE 4.17: Influence of δ_T on profile $\phi(\eta)$

effect on the temperature profile. While a higher δ_T led to a decrease in the temperature profile (as previously discussed), wich results in a decrease in the concentration profile, as well. This might be due to the delayed response of the nanoparticles to concentration gradients with a higher thermal relaxation time. The nanoparticles might take longer to adjust their distribution based on concentration variations within the fluid. Further investigation into the interplay between these parameters would be valuable for a comprehensive understanding of mass transfer processes in hybrid nanofluids.

Chapter 5

Conclusion

This investigation explored the influence of various physical parameters on the flow, thermal, and mass transfer characteristics of nanoparticles within two distinct fluids: a nanofluid (Al_2O_3/H_2O) and a hybrid nanofluid (Al_2O_3+Cu/H_2O). The parameters investigated included the unsteadiness parameter (β), magnetic field parameter (M), thermal relaxation parameter (δ_T), nonlinear thermal radiation parameter (Rd), Schmidt number (Sc), stretching parameter (λ), thermophoresis parameter (Nt), Brownian motion parameter (Nb), suction parameter (S) and activation energy parameter (E). Here is a summary of some key findings:

- Magnetic field (M) increases the temperature due to the Lorentz force hindering fluid motion and generating friction.
- Unsteadiness β and activation energy (E_a) potentially influence nanoparticle behavior, suggesting a rise in the concentration profile.
- Thermal relaxation time parameter δ_T exhibits a contrasting effect, with a higher δ_T leading to a decrease in temperature profile due to the delayed response of fluid particles to temperature changes.
- Thermal radiation (Rd) promotes a higher concentration profile through thermophoretic force.

Bibliography

[1] S. Choi and J. Eastman, "Enhancing thermal conductivity of fluids with nanoparticles," tech. rep., Argonne National Lab.(ANL), Argonne, IL (United States), 1995.

[2] R. Tiwari and M. Das, "Heat transfer augmentation in a two-sided lid-driven differentially heated square cavity utilizing nanofluids," *International Journal of heat and Mass transfer*, vol. 50, no. 9-10, pp. 2002–2018, 2007.

[3] M. Safaei, M. Gooarzi, O. Akbari, M. Shadloo, and M. Dahari, "Performance evaluation of nanofluids in an inclined ribbed microchannel for electronic cooling applications," *Electronics cooling*, vol. 832, 2016.

[4] S. Suresh, K. Venkitaraj, P. Selvakumar, and M. Chandrasekar, "Synthesis of $Al_2O_3 - Cu/H_2O$ hybrid nanofluids using two step method and its thermo physical properties," *Colloids and Surfaces A: Physicochemical and Engineering Aspects*, vol. 388, no. 1-3, pp. 41–48, 2011.

[5] I. Waini, U. Khan, A. Zaib, A. Ishak, and I. Pop, "Thermophoresis particle deposition of $CoFe_2O_4 - TiO_2$ hybrid nanoparticles on micropolar flow through a moving flat plate with viscous dissipation effects," *International Journal of Numerical Methods for Heat & Fluid Flow*, vol. 32, no. 10, pp. 3259–3282, 2022.

[6] A. Sharma, R. Singh, A. Dixit, A. Tiwari, and M. Singh, "An investigation on tool flank wear using Alumina/MoS_2 hybrid nanofluid in turning operation," in *Advances in Manufacturing Engineering and Materials: Proceedings of the International Conference on Manufacturing Engineering and Materials (ICMEM 2018), 18–22 June, 2018, Nový Smokovec, Slovakia*, pp. 213–219, Springer, 2019.

[7] S. Nadeem, N. Abbas, and A. Khan, "Characteristics of three dimensional stagnation point flow of hybrid nanofluid past a circular cylinder," *Results in physics*, vol. 8, pp. 829–835, 2018.

[8] A. J. Chamkha, A. Dogonchi, and D. Ganji, "Magneto-hydrodynamic flow and heat transfer of a hybrid nanofluid in a rotating system among two surfaces in the presence of thermal radiation and Joule heating," *AIP Advances*, vol. 9, no. 2, 2019.

[9] M. Khan, S. Qayyum, F. Shah, R. Kumar, R. P. Gowda, B. Prasannakumara, Y. Chu, and S. Kadry, "Marangoni convective flow of hybrid nanofluid ($MnZnFe_2O_4-NiZnFe_2O_4-H_2O$) with Darcy Forchheimer medium," *Ain Shams Engineering Journal*, vol. 12, no. 4, pp. 3931–3938, 2021.

[10] S. Nadeem and N. Abbas, "On both MHD and slip effect in micropolar hybrid nanofluid past a circular cylinder under stagnation point region," *Canadian Journal of Physics*, vol. 97, no. 4, pp. 392–399, 2019.

[11] M. Subhani and S. Nadeem, "Numerical analysis of micropolar hybrid nanofluid," *Applied Nanoscience*, vol. 9, no. 4, pp. 447–459, 2019.

[12] M. Izady, S. Dinarvand, I. Pop, and A. Chamkha, "Flow of aqueous $Fe_2O_3 - CuO$ hybrid nanofluid over a permeable stretching/shrinking wedge: A development on Falkner-Skan problem," *Chinese Journal of Physics*, vol. 74, pp. 406–420, 2021.

[13] B. Jabbaripour, M. Rostami, S. Dinarvand, and I. Pop, "Aqueous aluminium-copper hybrid nanofluid flow past a sinusoidal cylinder considering three-dimensional magnetic field and slip boundary condition," *Proceedings of the Institution of Mechanical Engineers, Part E: Journal of Process Mechanical Engineering*, p. 09544089211046434, 2021.

[14] W. Xia, S. Ahmad, M. Khan, H. Ahmad, A. Rehman, J. Baili, and T. Gia, "Heat and mass transfer analysis of nonlinear mixed convective hybrid nanofluid flow with multiple slip boundary conditions," *Case Studies in Thermal Engineering*, vol. 32, p. 101893, 2022.

[15] L. Crane, "Flow past a stretching plate," *Zeitschrift für angewandte Mathematik und Physik ZAMP*, vol. 21, pp. 645–647, 1970.

[16] S. Munawar, A. Mehmood, and A. Ali, "Effects of slip on flow between two stretchable disks using optimal homotopy analysis method," *Canadian Journal of Applied Sciences*, vol. 1, no. 2, pp. 50–68, 2011.

[17] I. Waini, A. Ishak, and I. Pop, "Unsteady flow and heat transfer past a stretching/shrinking sheet in a hybrid nanofluid," *International Journal of Heat and Mass Transfer*, vol. 136, pp. 288–297, 2019.

[18] S. Manjunatha, B. Kuttan, S. Jayanthi, A. Chamkha, and B. Gireesha, "Heat transfer enhancement in the boundary layer flow of hybrid nanofluids due to variable viscosity and natural convection," *Heliyon*, vol. 5, no. 4, 2019.

[19] M. Miklavčič and C. Wang, "Viscous flow due to a shrinking sheet," *Quarterly of Applied Mathematics*, vol. 64, no. 2, pp. 283–290, 2006.

[20] F. Tie-Gang, Z. Ji, and Y. Shan-Shan, "Viscous flow over an unsteady shrinking sheet with mass transfer," *Chinese Physics Letters*, vol. 26, no. 1, p. 014703, 2009.

[21] T. Fang, "Boundary layer flow over a shrinking sheet with power-law velocity," *International Journal of Heat and Mass Transfer*, vol. 51, no. 25-26, pp. 5838–5843, 2008.

[22] T. Fang and J. Zhang, "Thermal boundary layers over a shrinking sheet: an analytical solution," *Acta Mechanica*, vol. 209, no. 3, pp. 325–343, 2010.

[23] A. Rohni, S. Ahmad, and I. Pop, "Flow and heat transfer over an unsteady shrinking sheet with suction in nanofluids," *International Journal of Heat and Mass Transfer*, vol. 55, no. 7-8, pp. 1888–1895, 2012.

[24] M. Abel, N. Mahesha, and J. Tawade, "Heat transfer in a liquid film over an unsteady stretching surface with viscous dissipation in presence of external magnetic field," *Applied Mathematical Modelling*, vol. 33, no. 8, pp. 3430–3441, 2009.

[25] W. Ibrahim, B. Shankar, and M. Nandeppanavar, "MHD stagnation point flow and heat transfer due to nanofluid towards a stretching sheet," *International journal of heat and mass transfer*, vol. 56, no. 1-2, pp. 1–9, 2013.

[26] N. Abbas, S. Nadeem, A. Saleem, M. Malik, A. Issakhov, and F. Alharbi, "Models base study of inclined MHD of hybrid nanofluid flow over nonlinear stretching cylinder," *Chinese Journal of Physics*, vol. 69, pp. 109–117, 2021.

[27] E. Shaughnessy, I. Katz, and J. Schaffer, *Introduction to Fluid Mechanics*, vol. 8. Oxford University Press New York, 2005.

[28] R. Bansal, *A Textbook of Fluid Mechanics and Hydraulic Machines*. Laxmi Publications, 2010.

[29] S. Som, *Introduction to Heat Transfer*. PHI Learning Pvt. Ltd., 2008.

[30] J. Kuneš, "Thermomechanics," *Dimensionless Physical Quantities in Science and Engineering. Elsevier, Oxford*, pp. 173–283, 2012.

[31] J. Reddy and D. Gartling, *The Finite Element Method in Heat Transfer and Fluid Dynamics*. CRC press, 2010.

[32] B. Ishtiaq, A. Zidan, S. Nadeem, and M. Alaoui, "Scrutinization of MHD stagnation point flow in hybrid nanofluid based on the extended version of Yamada-Ota and Xue models," *Ain Shams Engineering Journal*, vol. 14, no. 3, p. 101905, 2023.